February 2016
Volume 122
Issue 1958
£5.60

www.electronicsworld.co.uk

Electronics WORLD

THE ESSENTIAL ELECTRONICS ENGINEERING MAGAZINE

SPECIAL REPORT
ANTENNA DESIGN:

- Performance analysis and test
- Improving signal reception
- High-gain metamaterials

New approach to IoT tools and kits
by Renesas Electronics

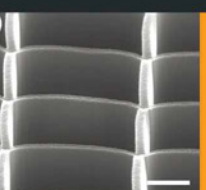

Technology
Nanotechnology shrinks new-gen optical devices

Power Conversion
Advantages of DSPs in the design of power converters

Products
Wide range of connectors and switches

Best of Class:
Parts in Stock Available for Immediate Shipment

Source: Distributor Evaluation Study, UBM Tech, May 2015

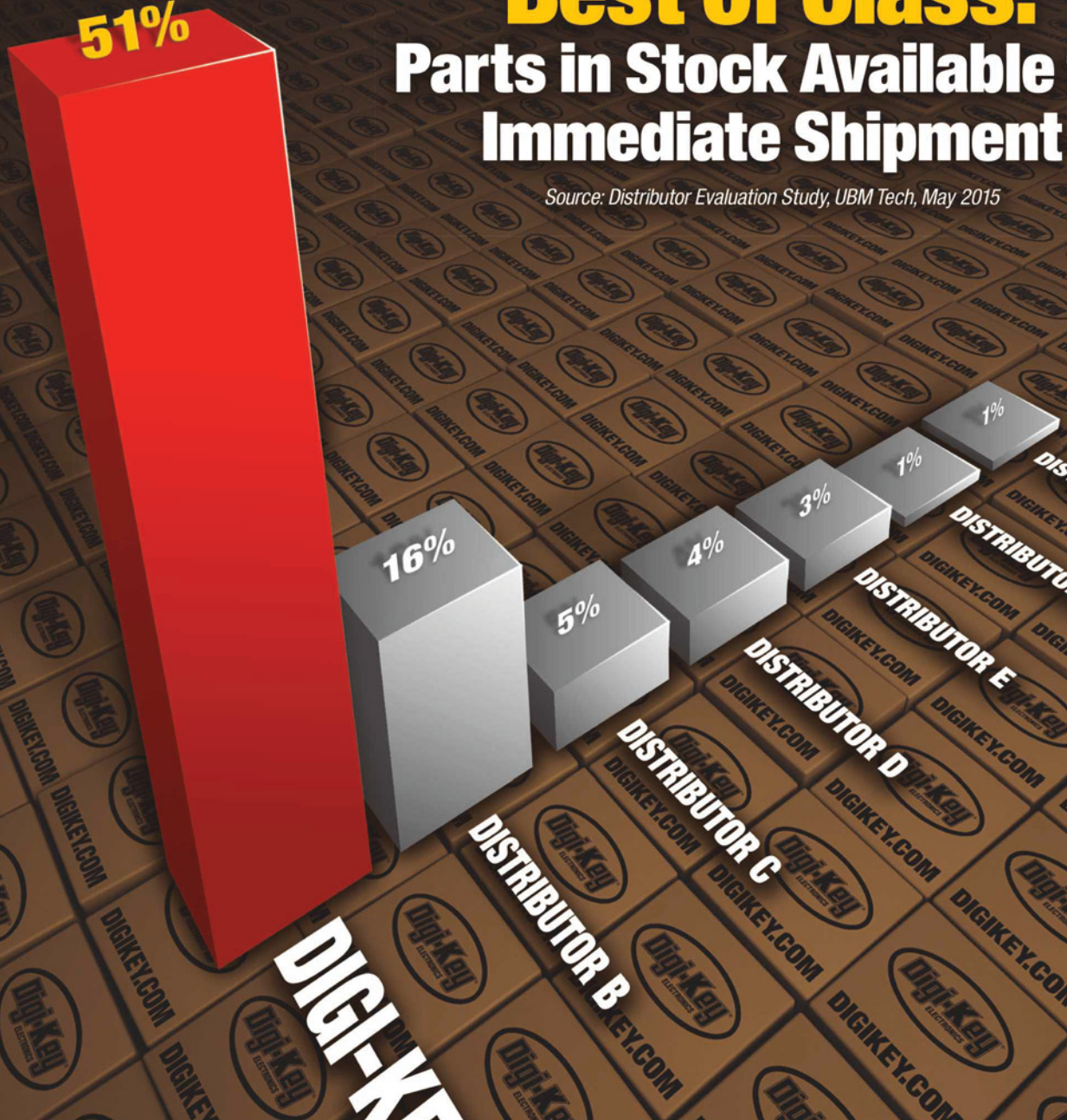

Digi-Key® ELECTRONICS

0800 587 0991 • 0800 904 7786

DIGIKEY.CO.UK

1,200,000+ PRODUCTS IN STOCK | 650+ INDUSTRY-LEADING SUPPLIERS | 4.6 MILLION PARTS ONLINE

*A shipping charge of £12.00 will be billed on all orders of less than £50.00. All orders are shipped via UPS for delivery within 1-3 days (dependent on final destination). No handling fees. All prices are in British pound sterling and include duties. If excessive weight or unique circumstances require deviation from this charge, customers will be contacted prior to shipping order. Digi-Key is an authorized distributor for all supplier partners. New product added daily.

ecia MEMBER ecsn member CEDA

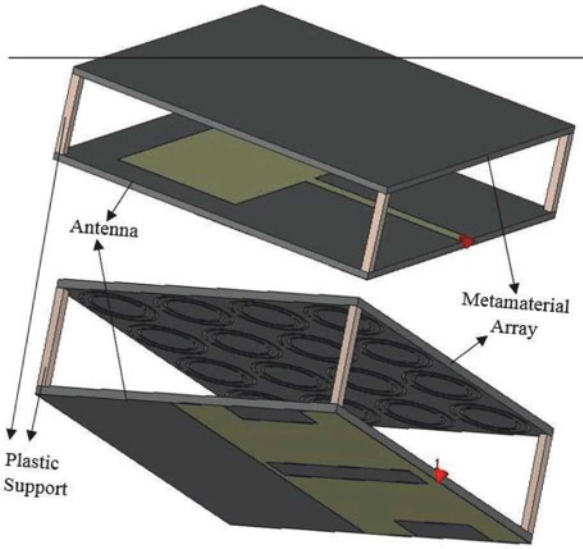

36

REGULARS

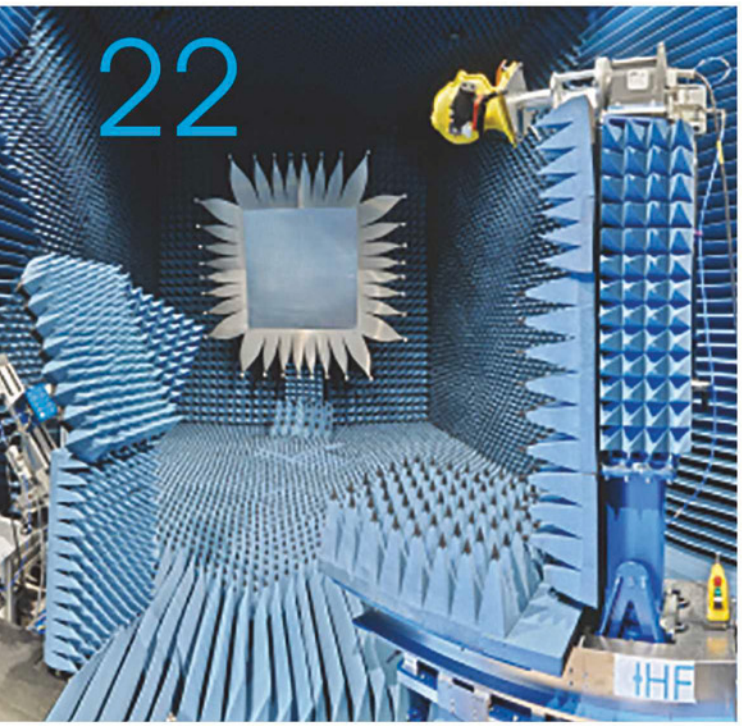

FEATURES

Cover supplied by RENESAS TECHNOLOGY EUROPE LIMITED
More on pages 8-9

Analog is Everywhere

Power Management

- DC/DC Conversion
- System supervisors
- Battery charging
- Power measurement

Interface

- CAN, LIN, USB, I²C, SPI, IrDA®
- Ethernet

Safety and Security

- Smoke Detection ICs (standard and custom)
- Piezoelectric horn drivers

Thermal Management

- Temperature sensors
- Fan controllers

Signal Conditioning

- Op Amps
- Comparators
- ADCs and DACs
- Digital potentiometers
- Instrumentation amps

LED Lighting

- Off-line
- DC/DC

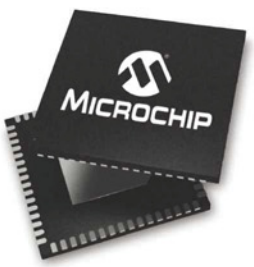

microchip DIRECT
www.microchipdirect.com

MICROCHIP

www.microchip.com/analog

E-TEXTILES WILL SEE RAPID GROWTH OVER THE NEXT DECADE

Whilst the majority of wearable technology products sold today still fit with the components-in-a-box design, 2015 was a record year for investment in smart clothing and e-textile products. To reach mass-market however, wearable technology must be useful, practical and fashionable, and seamless integration within textiles and clothing is seen as a key part of this.

There are still some challenges related to e-textiles, such as washability, durability, low cost and easy manufacture, which have left most of such projects restricted to low-volume niche products. This has started to change however, says industry analyst IDTechEx, who most recently found the market for pure e-textiles to be worth $100m in 2015.

In its latest market research report called *"E-Textiles 2016-2026"*, IDTechEx states that much of the focus is still on products in the sports and fitness sector and notably compression wear in the form of 'smart shirts'. Also, the market analyst firm states that whilst many of the largest players focus on these areas, there is significant interest and involvement from a wider range of sectors including the military, medical and healthcare, and workwear among others. Whilst the focus on 'smart shirt' biometric products has been undeniable, other applications include tracking specific physiological conditions beyond heart and respiration rate, the introduction of heaters, haptics and other actuators for rehabilitation or comfort, optimization of data and power wiring within apparel, and the integration of lighting or other visual features in apparel and home textiles alike.

IDTechEx predicts a significant impact in the e-textiles space when larger companies get involved. Initial entry-level players are apparel brands such as Adidas, UnderArmour and Nike, but others are expected to enter elsewhere in the value chain. Materials companies like DuPont, Nagase/EMS, Hitachi Chemical and others now offer specialised electronic materials for apparel. Electronics manufacturing giants like Flex and Jabil have started to invest heavily in this sector, the latter having acquired leading integrator Clothing+ in 2015. In addition, there is growing interest from Asia, where textiles giants from India, Sri Lanka, Taiwan and China are entering the market with large ambitions and deep pockets. The value chain involving assembly and volume production is soon expected to exist for a variety of diverse products.

> Whilst the focus on 'smart shirt' biometric products has been undeniable, other applications include tracking specific physiological conditions beyond heart and respiration rate

Examples of new technologies in this field, which still remain in research for now but will mature in the coming years, include e-fibres (RFID, sensing and more); new materials such as graphene, nanotubes and similar; energy-harvesting including photovoltaic, piezoelectric and triboelectric choices; energy storage in batteries and supercapacitors; and even logic and memory.

IDTechEx's report concludes that the market for e-textiles will exceed $3bn by 2026, up from $100m in 2015.

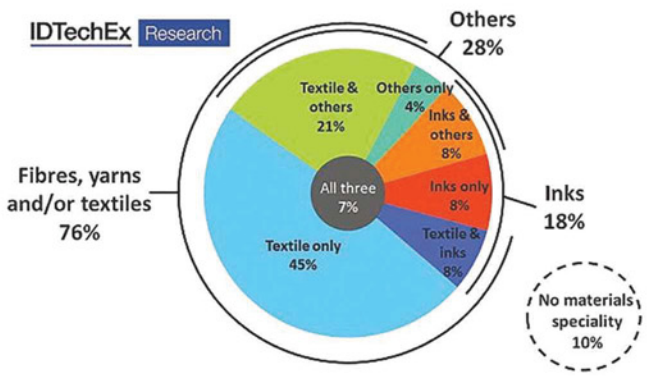

Percentage of e-textile players using each material type, derived from IDTechEx's survey of over 80 suppliers and manufacturers
[Source: IDTechEx Research report "E-Textiles 2016-2026"]

By James Hayward, Technology Analyst at IDTechEx, the independent research, business intelligence and advice organization (www.idtechex.com)

EDITOR:
Svetlana Josifovska
Tel: +44 (0)1732 883392
Email: svetlanaj@sjpbusinessmedia.com

SALES:
James Corner
Tel: +44 (0)20 7933 8985
Email: jamesc@electronicsworld.co.uk

Philip Woolley
Tel: +44 (0)20 7933 8989
Email: philipw@sjpbusinessmedia.com

DESIGN: Tania King

PUBLISHER: Wayne Darroch

ISSN: 1365-4675

PRINTER: Buxton Press Ltd

SUBSCRIPTIONS:
Subscription rates:
1 year: £65 (UK); £94 (worldwide)
Tel/Fax +44 (0)1635 879361/868594
Email: electronicsworld@circdata.com
www.electronicsworld.co.uk/subscribe

2nd Floor,
52-54 Gracechurch Street,
London, EC3V 0EH

Follow us on Twitter
@electrowo

Join us on LinkedIn

NANOTECHNOLOGY SHRINKS NEW-GEN OPTICAL DEVICES

A team of researchers from the University of Surrey's Advanced Technology Institute (ATI) have grown vertically-aligned carbon nanotubes (CNTs) in a grid-like formation on glass, which they believe will help miniaturize a range of optical devices. Removing the need for traditional curved, refracting lens systems, which are generally bulky and expensive, will create new, smaller and more flexible optical devices.

The nanomaterial can be transparent or opaque, depending on the angle the beam enters it, making it suitable for either collimating a beam of light or for absorbing stray light. This property will significantly improve line-of-sight applications such as optical data transfer or the rejection of stray light in high-specification space telescopes.

The next step is to incorporate the material into existing technology. ATI has already demonstrated low-temperature growth processes to enable direct wafer-scale integration of vertical CNTs with CMOS devices.

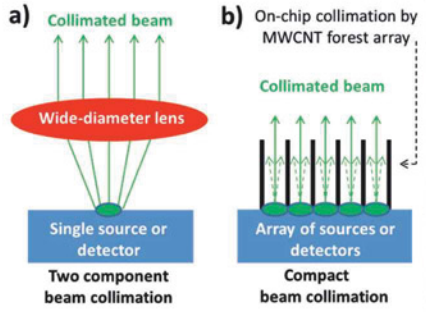

(a) Classical setup with a single light source and a single wide-diameter lens for collimation; (b) Suggested setup with an array of sources or detectors integrated with the carbon nanotube-based flat material for collimation

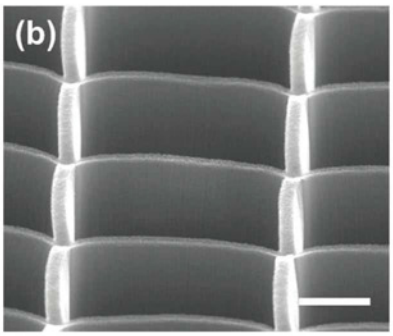

Scanning electron microscopy image of carbon nanotubes grown in a grid-like pattern on a glass substrate; 55° tilt and 15µm scale bar

RESEARCHERS ON TRACK FOR 'RACETRACK MEMORY' BREAKTHROUGH

New research from the Universities of Glasgow and Leeds on so-called 'racetrack memory' could be an important step toward creating faster, higher-capacity, lower-power data storage.

Unlike conventional hard disks which read data from a magnetized spinning disc, racetrack memory uses lines of stationary nanowires. Current passing through the wires creates 'domain walls' – spaces between the wires where information can be stored.

One key question still under investigation is the types of materials which will create the most robust data storage system, capable of storing and moving information quickly and efficiently.

The research team analyzed the structure of thin films deposited by sputtering from platinum, cobalt and aluminium oxide, which they believe may be suitable for racetrack memory. Tests have shown that this material allows data, encoded in spinning electrons, to travel up and down the walls at high speed.

ETRI PRESENTS BLUEPRINT OF A '5G FUTURE'

The Electronics and Telecommunications Research Institute (ETRI) of Korea held a 5G technology demonstration last December that showed a future social network service (SNS) and various 5G core technologies, including millimeter wave, Mobile Hot-spot Network (MHN) and in-band full duplex, among others.

"With this demonstration, we are officially introducing our R&D results on 5G," said Dr Hyun Kyu Chung, vice president of ETRI Communication. "We are trying to develop commercialization technologies needed by businesses, and to build a 5G ecosystem."

5G is the next generation wireless technology that promises high-quality videos of over 10Mbps served to 100 users simultaneously, even on a train running at 500km/h; users will experience data rates 100 times faster than those with current technologies.

ETRI's future SNS is a trial service model where 5G technologies will provide dynamic user-centric connection to people, things and spaces. It is characterized by instant content-sharing and Gbps-grade video applications in vehicles.

ZING is a near-field communication technology that enables mass data to be transmitted at rates of 3.5Gbps to devices within a radius of 10cm.

Single-RF-Chain compact MIMO technology enables a single antenna to simulate multiple antennas, reducing antenna volume and elliminating inter-antenna interference.

Millimeter wave (mmWave) beam-switching technology provides fast switching of radio beams to mobile users, allowing seamless Gbps-grade service in mobile environments.

Mobile Edge Platform (MEP) is a mobile edge cloud server on-board vehicles that will enable passengers to enjoy customized Gbps-grade content, connecting them to other users, things and spaces for user-centric services.

In-band full duplex technology can transmit and receive signals simultaneously over the same channel, doubling spectral efficiency.

Small-cell SW technology is designed for Access Point (AP)-sized small-cell base stations, reducing communication dead-zones and improving data rates per user in each hot-spot area.

Last month, ETRI demonstrated the Giga Internet service and future SNS in a Seoul subway train installed with MHN and ZING kiosks. ETRI also plans to introduce hand-over technology on a mmWave mobile communication system, and 5G radio access technology that satisfies the 1ms radio latency.

BEHIND EVERY SATISFIED CUSTOMER

THERE'S A DISTRIBUTOR YOU CAN COUNT ON

As the world's leading high-service distributor of electronics, automation and control, and tools and consumables, we do more than provide quality parts at competitive prices. With our dedicated customer service team who can offer technical support, as well as our award-winning design tools and resources, you can count on us for all the extra support you need.

uk.rs-online.com

COMPREHENSIVE RENESAS SYNERGY™ TOOLS & KITS SUPPORT ACCELERATES END-PRODUCT DEVELOPMENT

New approach to tools and kits meets the needs of today's highly-competitive IoT market

With marketgrowth projections going through the roof, the IoT market clearly offers tremendous opportunities. Innovative companies who can beat their competitors to market, successfully drive down total cost of ownership, and circumvent the typical barriers to entry will likely see success. Yet, the traditional approach to tool and kit support in the embedded MCU market is still filled with obstacles that block rapid prototyping and product development. MCU suppliers frequently require their customers to source development tools from multiple vendors, opening the door to a time-consuming and inefficient process.

The development kits that vendors offer often do not comprehensively address the needs for easeof- use and reliable expansion of connectivity and functionality. Embedded system developers, especially those bringing IoT products to market, are often forced to use software development tools with severe limitations on compiled code size unless extra fees are paid. Furthermore, many times these tools are typically not completely integrated with respect to MCU architecture and debugging options, operating systems and communication stacks, software maintenance and easy licensing, product documentation and project management.

Each of these factors contributes to longer development cycles, higher cost of ownership and missed market opportunities. IoT product developers need a platform that addresses all the development needs they encounter throughout the development life cycle of their end-products. The initial needs of this life cycle are very important . Development tools and kits must work together seamlessly without forcing developers to access multiple disparate resources before they become productive in their engineering tasks.

Clearly the key to success is a comprehensive Integrated Development Environment (IDE) that encompasses the total embedded solution and that is seamlessly paired with a scalable series of expandable development kits to meet the needs of a wide range of applications.

Full Featured Integrated Solution Development Environment (ISDE)

The Renesas Synergy Platform eliminates many of the limitations found in today's IDEs and MCU development kits. Renesas Synergy MCUs are supported by the Eclipse-based e2 studio tool for software development. Eclipse is the de-facto standard when it comes to embedded IDEs and, by adding new, solution-oriented components, Renesas' engineers have transformed this environment into a true Integrated Solution Development Environment (ISDE). As a standard Eclipse-based platform, the e2 studio ISDE can be readily extended in the future with tool components from Renesas and from third-party tool vendors as Eclipse plug-ins.

The following three capabilities – deep software debugging, clear trace visibility of real-time events within the context of a real-time operating system (RTOS), and intelligent guidance of MCU pin configuration – offer excellent examples of how Renesas' e2 studio ISDE provides unique solutionbased assistance.

Valuable Debugging Capabilities

The ISDE's debugging capability addresses a wide array of functions including simple breakpoints, single-step, instruction, data pattern targeting, CPU register display, and run control. With these functions, developers can quickly identify and fix errors by stepping through code from instructionto- instruction, viewing how the software performs and what errors lead to a bug. In addition, all of the Renesas Synergy Platform's development and starter kits feature an on-board version of the SEGGER J-Link® JTAG-based debugger that eliminates the need to purchase and connect external debugging probes. Viewed by many as a quasi-standard for ARM® Cortex®-M-based systems, SEGGER JLink ® is the most widely-used line of debug probes available today. To help accelerate code debug, the J-Link® features additional breakpoints for use when core-provided breakpoints are exhausted.

Deep Program Flow Tracing

The ISDE's tracing capability is a balance between real-time capture of data locally within the MCU device itself and post-processing this captured data externally within the ISDE tool. This gives the developer a historical view of the MCU's internal instruction flow and data manipulation with extremely high granularity. That capability provides insight into detailed software execution correlated to stimulus events that led to erroneous software behavior, including a view of what occurred just after the error.

The more data that can be captured in real-time on the MCU device, the better for full tracing. All Renesas Synergy MCUs have generous on-chip trace storage capability with 1KB trace buffers on the Renesas Synergy S1 and S3 Series MCUs and a 2KB trace buffer on the S7 Series MCUs. Through compression techniques, these buffer sizes can capture up to 64 instruction branches before needing to send trace data from the MCU device off to the ISDE. The S7 MCU devices go a step further by providing a streaming trace capability to bring out information in real-time during code execution. This capability enables developers to follow program flow as it steps through thousands of instructions and branches.

The Renesas Synergy Platform includes the comprehensive Renesas Synergy Software Package (SSP). The SSP offers developers a complete, qualified embedded software framework built around Express Logic's ThreadX® multitasking RTOS. To effectively aid development of complex real-time systems that have high-speed connectivity, the e2 studio ISDE integrates a high level of RTOS awareness. The Renesas Synergy Platform includes, at no charge, the use of Express Logic's host-based analysis tool TraceX® that gives developers detailed graphical visibility of real-time system events, allowing them to visualize how their system operates within context of the RTOS.

By tracking the occurrence of system events such as interrupts and context switches, TraceX® displays events graphically on the horizontal axis representing time, with the individual application threads along a vertical axis. Taken together with the ISDE's

traditional hardware debug capabilities, this extended visibility gives developers who are using the SSP tracing capability on both the MCU and RTOS levels.

Intelligent Guidance Speeds Project Startup

To simplify and automate configuration of Renesas Synergy MCU functions and code generation, the e2 studio ISDE offers many graphical configurators to guide user selections and prevent errors when starting a new design. Renesas Synergy MCU's can support many different functions (up to 16) on a single pin to provide complete flexibility during the layout design of a circuit board. The pin configurator guides developers to select the desired function of each pin graphically, checks for conflicts and suggests alternatives if needed, and documents the design for easy circuit board layout. The MCU system clock configurator guides the selection of correct clock sources and frequencies by performing dynamic validation during the selection process.

The RTOS configurator makes simple work of assigning and managing individual RTOS threads to tasks. Another configurator gives intuitive guidance to select optional operation of individual peripheral driver modules. A final configurator helps correctly assign interrupt sources to MCU interrupt inputs and prepares a total consistency check. At the end of the configuration process, the ISDE automatically generates C header files and initialization C source code reflecting all the choices to enable the developer to start writing application code immediately for the end-product.

Smart Manual

One of the more challenging problems developers face as embedded designs grow increasingly complex is how to efficiently manage and use the thousands of pages of documentation for MCU devices and software that accompany each design, especially in IoT applications. Developers can spend many extra hours trying to track down the information they need.

To address this problem and simplify development, the e2 studio ISDE for Renesas Synergy uses an innovative new feature called Smart Manual, which is part of the overall Smart Documentation system in the Renesas Synergy Platform. As an interactive source of assistance within the ISDE, the Smart Manuals is context-aware meaning it presents the user with information that is needed, when it's needed. For example, if a developer is writing application code and wants to know more detailed information about a particular MCU register or a particular API function call within the SSP, as he or she moves the cursor over each MCU register name or software API, the tool pops up the associated details for structure, bit definition, parameter types, and more. When the engineer clicks on this information or accesses help, a context-aware link to additional information associated with that particular feature appears. The system even collects relevant application notes and media-rich instructional material associated with the topic in question. The Smart Manual saves time by eliminating the need to search resources outside of the e2 studio ISDE.

Renesas Synergy Development Kits and Starter Kits

To ensure immediate start-up and smooth development all the way to the prototype stage, it is very important that the software development environment is tightly coupled with the MCU development kits. Planned from the outset, the e2 studio ISDE is structured to work seamlessly with a wide range of kits for the Renesas Synergy Platform to match the varying technical expertise of users and varying complexity of different end-applications. There are pre-configured board support packages (BSP's) available in the ISDE for each Renesas Synergy kit for immediate start up and easy modification to expand and alter the functionality of the kits.

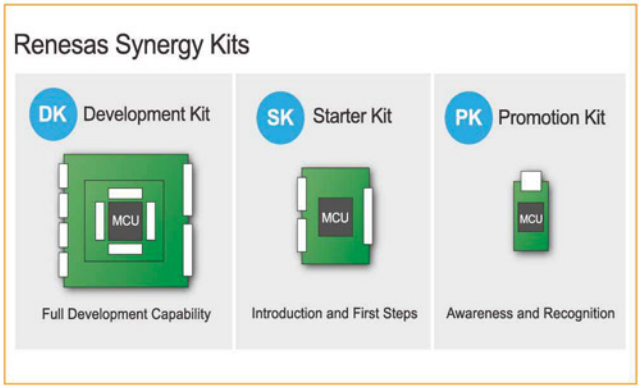

Renesas Synergy Development Kits, also known as DK's, are available for every series of Renesas Synergy MCUs. DKs enable full access to all the MCU features and pins to evaluating MCU device performance and measure power consumption; build application software until the end-product's prototype hardware development platform is available; and even to expand capabilities by plugging specialized circuit boards into DK expansion connectors including industry standard Pmod™ connectors. To make the evaluation and development process more geared towards software developers, Renesas Synergy DK's also feature active multiplexers on the GPIOs that allow developers to dynamically configure the signals with just a single switch, setting rather than manually setting many tiny jumpers that can cause errors and consume time. Renesas Synergy Starter Kits, or SK's, offer high value at a very affordable price. These basic kits provide an excellent introduction to the Renesas Synergy Platform while addressing the vast majority of Renesas Synergy MCU functions. SKs are targeted at developers who may not have a specific application in mind yet, but want to try out the Renesas Synergy Platform at minimal cost. Each SK provides access to most MCU pins and also provides function expansion through sets of connectors based on the Pmod™ standard and on the Arduino™ format for Arduino™ Shield plug-in boards.

All Renesas Synergy DK's and SK's include J-Link® on-board (J-Link® OB) JTAG debug access using a simple USB connection.

Conclusion

Today's embedded and IoT applications demand a comprehensive development suite that integrates the capabilities of an ISDE with an extensive selection of hardware kits. At the same time, developers need tools that are not only productive, but also easy to use. By combining new capabilities such as a context-aware smart manual, automated project configuration, RTOS awareness, and enhanced tracing functionality, Renesas has given Renesas Synergy Platform users the tools they need to rapidly develop exciting new embedded applications and beat their competitors to market.

About Performance...

BY **LUCIO DI JASIO**, MCU8 BUSINESS DEVELOPMENT MANAGER AT MICROCHIP TECHNOLOGY

Not long ago, I attended a hands-on workshop on introducing a group of millennials (people reaching young adulthood around the year 2000) with a foundation of computer science to the art of embedded programming. Sure enough, one the first examples was the "Hello Embedded World" project which – of course! – meant blinking an LED.

The instructor did a pretty good job of avoiding being side-tracked, and guided the class through the project by starting with a simple I/O port to target with the simplest possible solution. This meant a pair of blocking (waiting) loops and two assignments that, he explained, were sure to be turned into MCU instructions (bit-set and bit-clear) by the clever C compiler. Soon, the room was filled by the intermittent light from many small red LEDs which, much to the presenter's disappointment, the crowd did not seem too enthusiastic about.

From the back of the room I started listening to the grumble. Soon, the source of the group malcontent was revealed: as often is the case, it was a matter of incorrectly set expectations. There is blinking and then there is pulsing or breathing, as modern Mac (and many other mobile device) users know their devices do when in standby. Ah, thanks for that Apple!

Running Short On MIPS

From there the class took an unexpected turn as the presenter tried to accommodate the audience and went off on a tangent to introduce the relative complexity the new task entailed. A timer had to be introduced and, with it, pulse width modulation (PWM) could be arranged to adjust the luminous output of the LED by controlling its duty cycle.

Next, he explained how this had to change gradually, through a number of steps up and down a ramp defined in a table. The timing of each step required yet another (slower) timer, which produced an interrupt. The MCU would respond to this interrupt and compute (or consult a lookup table) to assign a new duty cycle value to the PWM. This was already too much for the audience on their first foray into the world of embedded design, but things got worse as he tried to impress them with a quick back-of-the-envelope calculation.

Here are the maths steps as I recall them:

- Choose a PWM period such that we can count on the human eye's persistence effect: 30 ~ 120Hz.
- Then multiply that value to provide a smooth dimming effect with, say, 256 steps, which gives ~ 32kHz. So far so good, since there is an extremely low-power internal oscillator available inside each PIC microcontroller running at exactly that frequency.

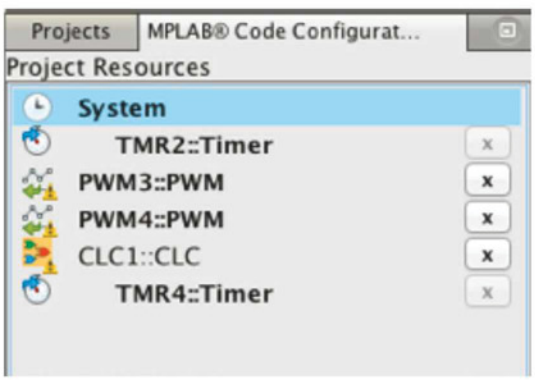

Figure 1: MCC "Project Resources" window

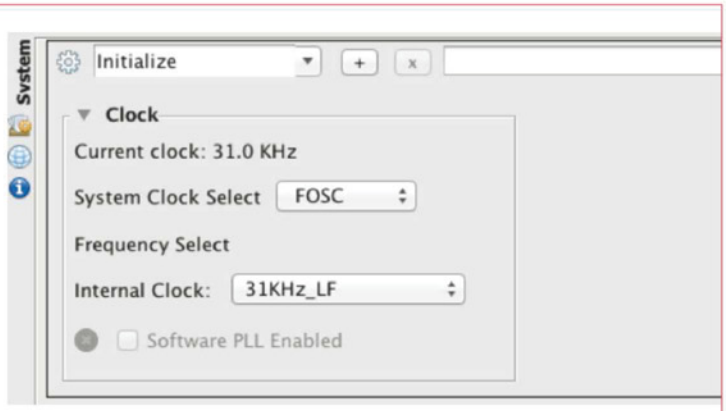

Figure 2: MCC System configuration window; clock detail

Figure 3: MCC system configuration window; Config Bits detail

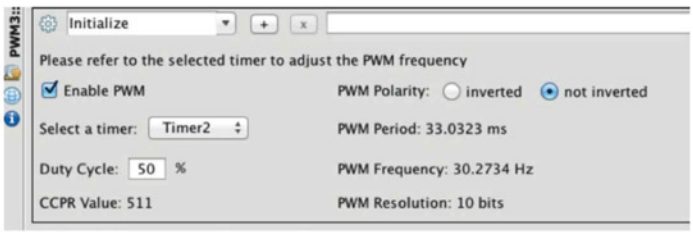

Figure 4: PWM3 configuration window

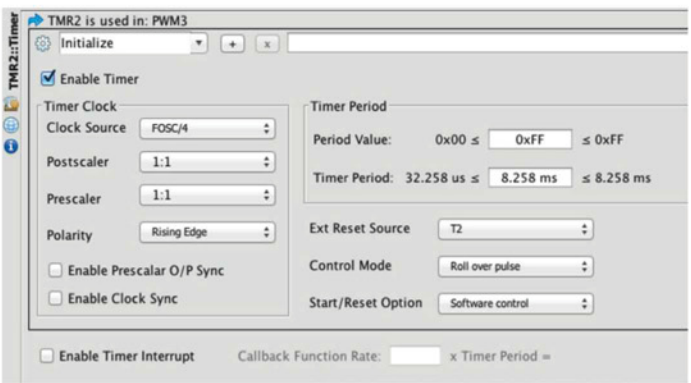

Figure 5: TMR2 configuration window

● Now, if we want to produce the simplest breathing effect (using a triangular profile) with a period between ½ second and 2 seconds, we will need to ramp up and down 512 (total) steps in each period. This translates roughly into updating the PWM approximately each millisecond. In MCU-cycle terms, at the 32kHz clock frequency we would receive one interrupt every eight instruction cycles. Even to the most inexperienced embedded designer that sounded an impossible proposition. The clock rate had to be increased, or in other words, we were running short of MIPS!

This was quite a realization for some in the audience, as for the first time they understood that the term performance (as in MIPS and MHz) had a very different meaning in this context. We needed to push the microcontroller faster, even though we were not even attempting any calculations; we just needed timely response to an event! This was their first encounter with the concept of real-time performance.

Feel The Beat

The exercise resonated with me as well, and that's why I write about it here. I had been looking for simple ways to illustrate the limitations of the traditional MCU/core-centric approach to embedded applications. Today, we are obsessed with performance, MIPS, MHz and megabytes, yet we often focus on the wrong type of performance.

Sometimes, stepping back and looking at a problem from a new angle can reveal a hidden, more elegant and balanced solution. For example, when you approach the breathing LED problem presented here, but free your mind from the chains of the MCU/core-centric culture, you notice a striking similarity between the visual LED pulse and the acoustic effect produced by the "beating" of two combined periodic signals of close frequency as they add and cancel. The sum of the two reaches our ears with an envelope that is recognizably periodic, and with frequency equal to the difference between the two. That is not difficult to implement with just a couple of logic gates and can be done within a microcontroller with the right type of peripherals.

Core-Independent Solution

To implement this, first we need to find a way to generate two periodic signals (square waves are ok) with frequency only 0.5-2Hz apart. A pair of digital timers with a reload register (basic PWM peripherals) can be used to create the two signals. We need to carefully choose the two reload frequencies to be close but different to produce the desired beat frequency. For example, if we use a PIC microcontroller with a clock at 32kHz, two 8-bit timers and the connected PWM modules can generate 30.5Hz and 31.5Hz outputs. We can then use one of the configurable logic cells, or CLCs – a small programmable logic blocks similar to FPGA/PLD macro blocks, to perform logic 'and' on the two signals. Eventually, we can send the output of the CLC directly to any of I/O pin where an LED is connected. This will give a visible breathing effect of ~ 1Hz.

Faster breathing can be achieved by increasing the difference between the two frequencies (making the second PWM period shorter) and, vice versa, slower breathing is achieved by reducing the difference between the two all the way to ~ 0.1Hz, when the two reload registers are only one count apart.

The CLC is the most basic of the Core Independent Peripherals found inside modern (PIC) microcontrollers, and for the rest of the solution we have used only standard issue timers (PWMs).

You might wonder if, at this point, we had no more use of the MCU itself! In fact, the microcontroller core is used during the

power-up of the application to configure the peripherals. Perhaps even more interestingly, we have reached our solution using our lowest power consumption oscillator, leaving 100% of the microcontroller performance (MIPS, MHz, whatever) available for use at "other", hopefully more interesting, tasks!

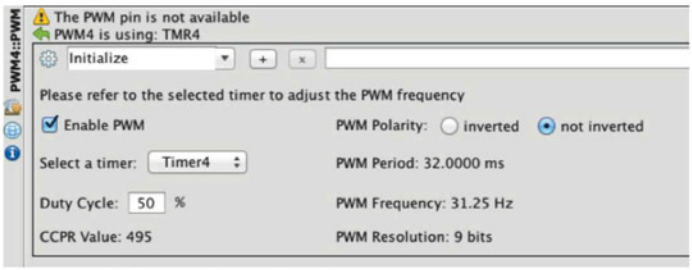

Figure 6: PWM4 configuration window

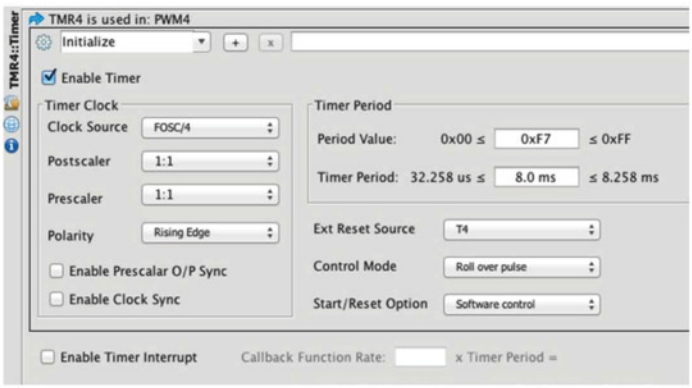

Figure 7: TMR4 configuration window

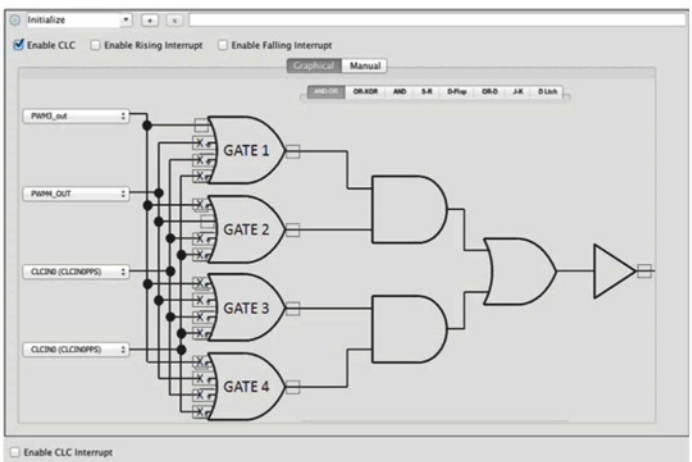

Figure 8: CLC1 configuration window

Look Ma, No Code!

If that sounds great, you will be even more pleased to learn how to put this into practice without opening a datasheet or writing a single line of code.

For simplicity, I will use the PICDEM Curiosity board, but any other board that hosts a 14/20-pin PIC micro will do. I use the PIC16F1619, which is conveniently shipped with the board (although it is socketed and easily replaced).

I'll also use the MPLAB X IDE "New Project" wizard to create a new project with the selected PIC model, and the MPLAB Code Configurator v2.52 (a free plugin) to initialize and connect all the peripherals. They can simply be picked out of the "Device Resources" list by double-clicking on their names.

In our case, we double-click on PWM3 and PWM4, and one of the CLC modules – I picked CLC1.

In the top window, where the selected "Project Resources" are listed (see Figure 1), we can click on each and inspect their configuration dialog windows. It is here we learn the specific options available for each resource.

Always on top of the list is the "System" item, which represents the essential elements of the microcontroller, such as various oscillators and the configuration bits. Set the oscillator to the "31kHz_LF" mode (which is the lowest power of all), as shown in Figure 2, and a few lines below remember to enable the "LVP" configuration bit as shown in Figure 3. This is required for the Curiosity board's built-in PIC programming circuit to operate correctly.

> "Today, we are obsessed with performance, MIPS, MHz and megabytes, yet we often focus on the wrong type of performance

Next, click on the PWM3 resource (see Figure 4). You will notice that a timer has already been selected as its time base; by default this is Timer 2. So, MCC has already added it to the list of "Project Resources" and we proceed there to configure it, as all other options are already set as needed (by default); these include a duty cycle of 50% and non-inverted output polarity.

Clicking on TMR2 (see Figure 5), we are once more presented with a number of sensible default values, including the period value already set to 0xFF (255).

Click on PWM4 now (see Figure 6) and change the time base to Timer 4, so we can select a different period. As soon as you do that, you will see TMR4 appear on the list of Project Resources. Click on it as well, but now change the period value to 0xf7 (247) as shown in Figure 7.

Finally, click on the CLC1 module and configure the first two input signals to be connected to the PWM3 and PWM4 outputs respectively (see Figure 8). Connect them to GATE1 and GATE2, and ensure the "AND-OR" function is selected.

Next, use the "Pin Manager" button to access the I/O configuration table where you must assign a pin to the CLC1

output: RA2 in our case, which is physically connected to one of the four LEDs on the Curiosity board.

Pressing the "Generate Code" button will trigger the MCC into action producing a set of six small source files (written in C), providing all the necessary peripheral initialization code. In fact, MCC will also volunteer to create a main file, which we will accept gladly, and this will add a "main.c" file, containing calls to the peripheral initialization and an empty main loop.

Don't be surprised if at this point I tell you to simply ask MPLAB X to build the project and program the Curiosity board with a single last click on the "Make and Program" button.

After a few seconds for the compiler, linker and programmer to do their job, you will be happy to see the little Curiosity board LED breathe!

In Less Than 10 (Binary) Lines Of Code

Contrary to the last part of this series (*"In 10 Lines Of Code"*, EW, January 2016), this time we did not have to manually type a single line of code. By simply combining a few (core-independent) peripherals to build a new function, we got things done and we still have 100% of our MCU performance available for use in the rest of our application. ●

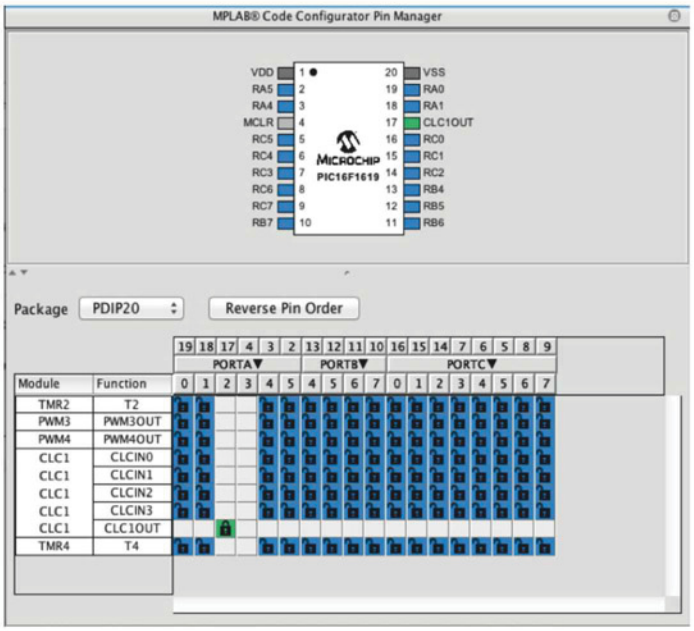

Figure 9: MCC "Pin Manager" window

Using biotelemetry in medical care

BY **DR DOGAN IBRAHIM**

Biotelemetry – or medical telemetry, or wireless medical telemetry – is the application of radio telemetry techniques for remote monitoring of patients' physiological parameters, such as blood pressure, pulse rate, respiration rate, blood oxygen concentration and so on.

In a typical hospital-setting biotelemetry application, wireless sensors are attached to the patient, transmitting data on a continuous basis to nurses' station or other centralized receiving stations, even when the patient is mobile. This setup enables medical staff to keep an eye on multiple patients simultaneously from a fixed location.

The ability to remotely monitor a patient's vital signs in real time is very topical at present, for medical personnel and researchers alike. One of the aims is to allow the patients their mobility and, hopefully, a speedier recovery in their home environments. It is known that living as normal a life as possible in the home environment makes the patients feel secure, an important aspect of their recovery. Current and emerging advances in medical sensor technology and wireless communications have enabled the monitoring of non-critical patients in their own homes.

Here we describe the design of a microcontroller-based biotelemetry system for transmitting person's blood pressure and pulse rate to a monitoring receiving station, in this case a PC. The communication uses a pair of UHF TX/RX radio-telemetry modem modules.

Biotelemetry System Components

A typical biotelemetry system consists of the following components:

- Sensors suitable for monitoring medical parameters;
- A mobile (battery-operated) transmitter unit with processing capabilities;
- A receiver unit with processing capabilities for displaying data, preferably from multiple patients.

Sensors are a vital component of all biotelemetry systems. Although, in general, most industrial and commercial sensors can be used in medical applications, we now have a new generation of smart sensors developed specifically for medical healthcare. They are usually complex microchip-based devices that combine sensing with data processing in a single integrated circuit.

The main requirements for medical sensors include small size, low weight, robustness, water resistance, wide temperature range, low power consumption, high reliability and high accuracy.

Transmitter/Receiver Modules

For the RX/TX modules, the choice of wireless technology depends on the system developer; this could be Bluetooth, Wi-Fi, ZigBee or basic RF. The first three are well-known and established protocols, using high-level encryption algorithms. However, Bluetooth and ZigBee are not widely used in

Figure 1: Basic biotelemetry system setup

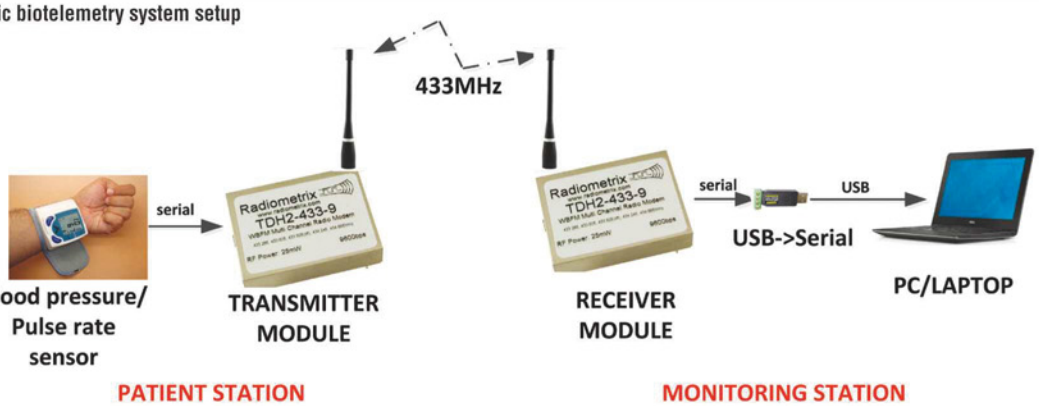

biomedical radio telemetry applications.

Basic RF provides wireless radio telemetry-based communication in the VHF/UHF bands. The licence-free industrial, scientific and medical (ISM) bands are commonly used, but different countries have allocated different frequencies for ISM, such as 902-928MHz and 2.4-2.4835GHz in the US, and 431.1-434.8MHz and 868-868.6MHz in Europe. However, none of these bands are exclusive to biomedical telemetry equipment and are heavily used by a wide variety of devices, making the medical equipment susceptible to electromagnetic interference.

Because of spectrum crowding, many countries have started to allocate frequency bands exclusively for biotelemetry use; one such example is the Wireless Medical Telemetry Service (WMTS). In the US, WMTS falls within the 608-614MHz, 1395-1400MHz and 1427-1432MHz bands, specifically approved for all biomedical communications except video and voice, protecting medical equipment from interference caused by other sources. Although some companies still use Wi-Fi and Bluetooth for their wireless medical telemetry devices, in the US the FCC actively encourages the use of WMTS instead.

Data Security And Integrity

Data security and data integrity are very important in medical telemetry systems, ensuring that what's transmitted is actually what is received at the other end of the system. Any errors must be detected and corrected before becoming part of the patient's medical record.

The system should be designed to minimize all kinds of electromagnetic interference. Transmitting incorrect data can have very serious health implications, causing emergency actions to be taken unnecessarily. In addition, transmitting personal medical data carries privacy concerns, so the data must be protected from unauthorized access. In most cases this can be achieved with password protection and/or encryption techniques.

Speed is another important factor in real-time medical monitoring, where data should be received reliably in a timely manner.

Example Biotelemetry System

The setup of a basic biotelemetry system is shown in Figure 1. At the Patient Station, a wrist-worn biomedical sensor captures data such as blood pressure and pulse rate. An RF radio telemetry transmitter module sends this data to the Monitoring Station, a compatible RF radio-telemetry receiver, which then passes it on to a PC to display in real time.

Figure 2 shows the system block diagram. The blood pressure and pulse rate sensor used in the project is supplied by Sunrom Technologies (www.sunrom.com). This is a standard digital blood pressure measuring device, providing RS232-compatible output to the host computer output to the data link.

Figure 2: System block diagram

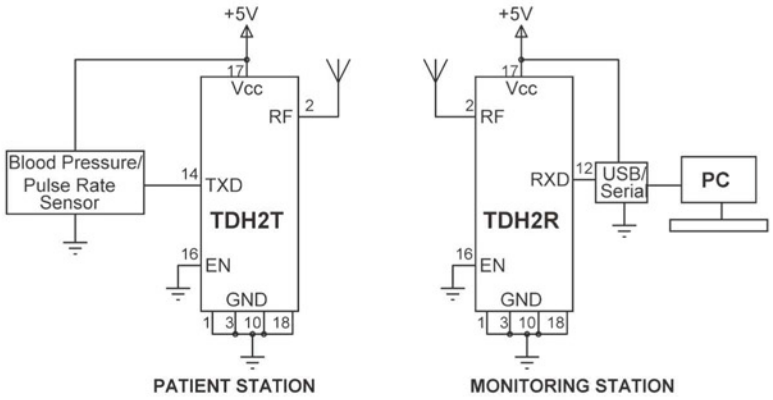

Figure 3: Displaying the parameters using ListBoxes

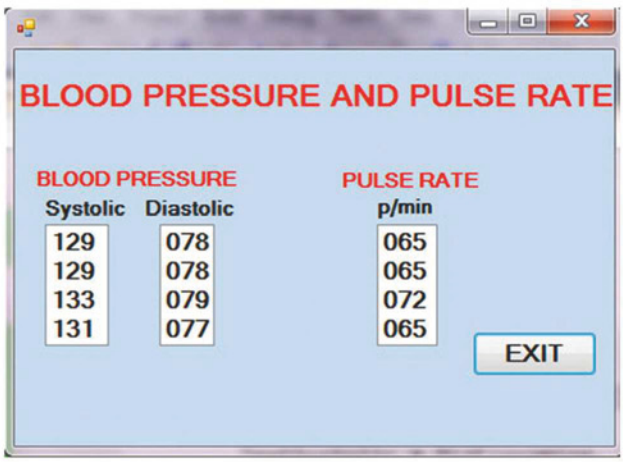

The Software

The desired normal blood pressure values are nominally 120mmHg systolic and 80mmHg diastolic, respectively. Although pulse rate varies in different people, the desired normal range in a healthy person is 50-80bpm.

The blood pressure and pulse rate sensor output is in ASCII in the following format:

<CR>sss, ddd, ppp<LF>

where sss and ddd are the systolic and diastolic blood pressure readings respectively (in mmHg), and ppp is the pulse rate every minute.

The PC software is based on Visual Studio, Visual Basic. The measured parameters are displayed using ListBoxes as shown in Figure 3.

Figure 4 shows the complete PC software listing. The main program executes continuously in a 'Do While' loop, where the serial data is read into variable incoming. The systolic and diastolic

pressure values and pulse rate are extracted and displayed in ListBoxes 'Systolic', 'Diastolic' and 'Pulse' respectively.

Our example system is very simple, but in real applications a medical telemetry system may receive wireless data from a number of different sensors and from several patients at the same time, needing further processing for added security, reliability, data integrity and indication of various health conditions.

In general, the following scenarios are possible: (a) single patient, single sensor; (b) single patient, multiple sensors; (c) multiple patients, multiple sensors. A radio telemetry module may offer multi-channel features for use in the case of multiple patients. For example, sensor data from several patients can be transmitted into multi-channel modules; a single multi-channel receiver module can request data from all the used channels, and then process and display it accordingly. Such multi-channel applications may require two-way communication using transceiver modules rather than simple transmitters and receivers. ●


```
Imports System.IO.Ports

Public Class Form1
 Public mySerialPort As New SerialPort

          Private Sub Form1_Load(sender As System.
          Object, e As
                    System.EventArgs) Handles MyBase.
                    Load
          Dim incoming As String
          Dim TextSystolic As String
          Dim TextDiastolic As String
          Dim TextPulse As String

          With mySerialPort
                    .PortName = "COM36"
                    .BaudRate = 9600
                    .DataBits = 8
                    .Parity = Parity.None
                    .StopBits = StopBits.One
                    .Handshake = Handshake.None
                    .Open()
          End With

          Me.Show()
          Do While (1)
           incoming = mySerialPort.ReadLine()
           If Len(incoming) = 14 Then
          TextSystolic = Mid(incoming, 2, 3)
          TextDiastolic = Mid(incoming, 7, 3)
          TextPulse = Mid(incoming, 12, 3)
          Systolic.Items.Add(TextSystolic)
          Diastolic.Items.Add(TextDiastolic)
          Pulse.Items.Add(TextPulse)
          Me.Refresh()
 End If
 Loop
          End Sub

          Private Sub ButtonExit_Click(sender As System.
          Object, e As
 System.EventArgs) Handles ButtonExit.Click
          mySerialPort.Close()
          End
          End Sub
End Class
```

Figure 4: PC software listing

IMPROVED SIGNAL RECEPTION WITH ANTENNA DIVERSITY, USING MULTIPLE HIGH-SPEED DACS

BY **CLARENCE MAYOTT**, APPLICATIONS ENGINEER FOR MIXED SIGNAL PRODUCTS AT LINEAR TECHNOLOGY

In modern wireless systems, numerous diversity techniques are used to maximize data throughput and improve transmission reliability. Time, frequency and code diversity techniques are used to transmit signals to multiple users simultaneously and to maximize the amount of data transmitted. By transmitting at different times on different frequencies, or with different binary sequences known as Gold codes, signals are produced that can be differentiated from each other and received error-free. These techniques are widely known and have been perfected over decades.

These techniques can also be used with antenna diversity or spatial diversity. Antenna diversity involves using multiple antennas to transmit or receive a signal. Simple antenna diversity chooses the antenna combination with best performance to decode a signal.

More complex versions of antenna diversity include MIMO (multiple input, multiple output) systems and beamforming applications, where multiple antennas are used at the transmission and receiving ends to increase spatial diversity.

With multiple broadcasting antennas it is critical to have timing variation in the picosecond range between the digital-to-analog converters (DACs) on each channel. This requires DACs that can be synchronized so the transmitted data is broadcast simultaneously. With this condition met, the system will be able to transmit identical data over multiple antennas to a common receiver, maximizing accurate signal reception and minimizing signal drop-offs from the transmitter.

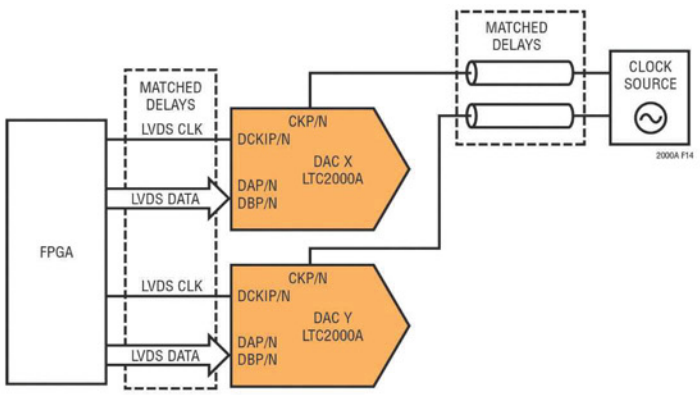

Figure 1: System with multiple LTC2000A DACs synchronized

TDMA, FDMA, CDMA

Communication systems can handle multiple users with diversity. The most basic version of this is time division multiple access (TDMA), which essentially involves transmitting data to multiple users at different times. The receiver then simply waits for its time slot to decode the appropriate data.

Frequency division multiple access (FDMA) works in much the same way but in the frequency domain. Data is transmitted to different users on specified frequencies and the receiver decodes data only on those frequencies.

More modern systems incorporate code division multiple access (CDMA) into wireless systems where the transmitted data is convolved with a specific code before it is transmitted. This same code is then used at the receiver to only decode data sent to that specific user.

Since these techniques are implemented in different domains, they can be used together in the same system for maximum diversity.

These techniques address an unavoidable effect when transmitting data over any distance, known as fading. Fading occurs when a signal decreases in amplitude due to cancellation in the transmitting channel. From a broadcasting antenna, the signal will undoubtedly take several different paths on its way to the receiver and in the process also change its phase. These differences in phase can potentially cancel the signal at the receiver, causing fading.

To counteract fading, multiple transmit or receive antennas can be used, as the likelihood of a signal sent or received on multiple antennas being cancelled is very low.

Antenna Diversity

Antenna diversity is one way of implementing spatial division multiple access (SDMA), since the physical space between antennas is used to distinguish between signals. There can be multiple antennas on the transmit side and a single antenna on the receive side (MISO); a single transmitting antenna and multiple receiving antennas (SIMO); or, multiple transmitting antennas and multiple receiving antennas (MIMO).

MIMO-based systems offer the best results in terms of antenna diversity, but the complexity of the decoding requires a sophisticated transmitter and receiver. In an environment

that is constantly changing, constant channel characterization is required. Also, as the distance between transmitter and receiver increases, the complexity of the channel between the transmitting and receiving antennas increases and becomes unstable and difficult to differentiate, making the benefits of MIMO less pronounced.

Systems with multiple transmitting antennas and a single receiving antenna are quite common in wireless communications and reply on antenna diversity to improve performance.

In a MISO wireless system with antenna diversity, multiple DACs transmit data on multiple antennas simultaneously. Since transmitting antennas are at physically different locations, on a tower for instance, their signals will propagate to the receiver in different ways. The paths from each transmitting antenna to the receiving antenna will be different, due to the different multipath effects in each channel. Characterization of each individual channel with transmitted pilot tones gives the receiver valuable information on the performance of each channel. This information can be relayed back to the transmitter and used to digitally modify the data before transmission, maximizing the likelihood of reception at the receiver.

Since each channel requires specific modification and correction, separate DACs and a dedicated digital signal processor (DSP) are required for each transmitting antenna. If the transmitting DACs are not perfectly aligned in time, the transmitted signals will be misaligned and beamforming accuracy will be poor. The transmitter will be unable to maintain a stable channel from point to point, and the receiver will be unable to correct for these errors.

To avoid this in the time domain, the DACs need to be synchronized, meaning the data must be transmitted from each DAC at an identical time, as even the slightest variation in time can degrade performance of the system.

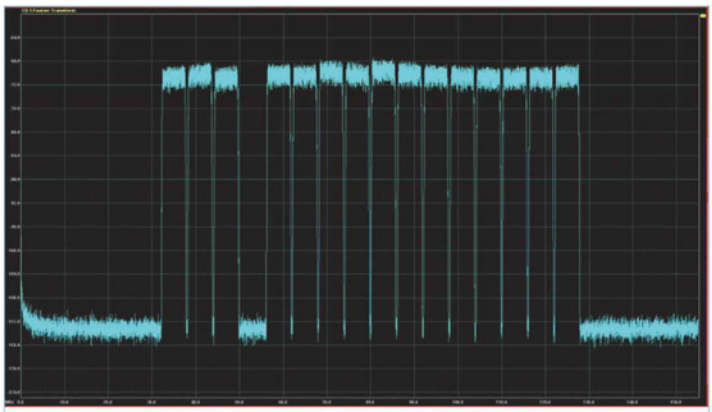

Figure 2: Frequency domain plot showing 16 channels of CDMA, produced by the LTC2000A with a single-gap channel

Synchronization

When DACs output data at gigahertz speeds, it is extremely difficult to synchronize their outputs across multiple devices. If a DAC is sampling at 2.7Gsps, the output code is changing every 370ps. The FPGA's sample and data clocks need to be aligned for each of the transmitting DACs. However, there are devices, such as Linear Technology's LTC2000A, that simplify synchronization.

LTC2000A is a 2.7Gsps, 16-bit DAC with an internal register that adjusts the latency of the data through the DAC. To use this feature, the timing mismatch between the data and clock lines for each DAC must be within 0.4 cycles of the sample clock frequency. Figure 1 shows the ideal routing of two LTC2000A devices. The data and clock paths' trace lengths to individual DACs need to match within picoseconds, achieved through

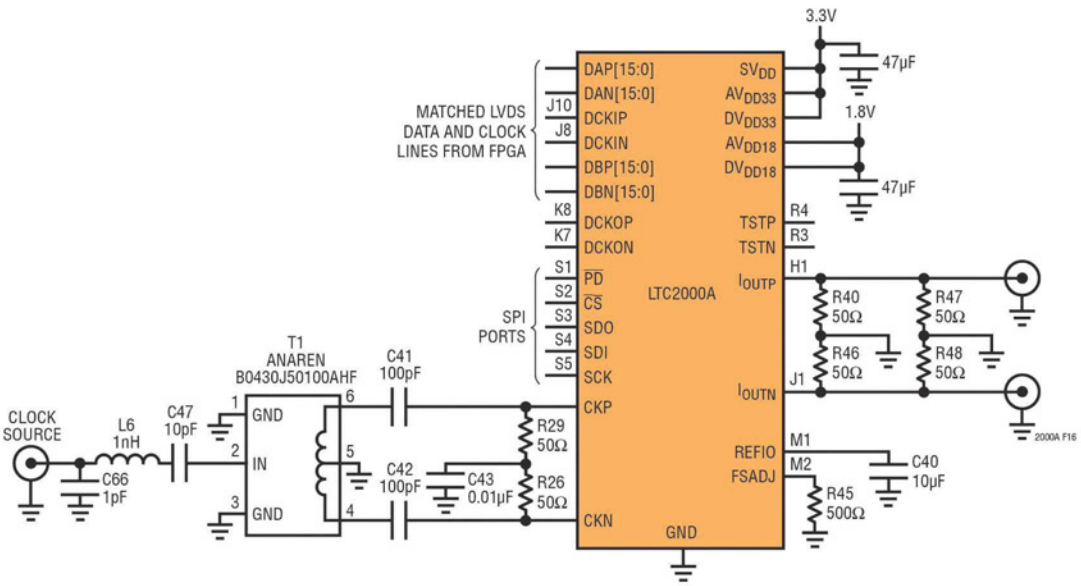

Figure 3: Typical schematic for implementing LTC2000A

digital routing techniques. If these criteria are met, then the data is guaranteed to be within one cycle from device to device.

An internal register within the LTC2000A programs the latency of data pipeline. Each DAC register can be individually set, which will ultimately align all the DACs in time domain, guaranteeing maximum performance when all diversity techniques are used. Increasing the number of transmitting DACs also increases the possible diversity. The ability to synchronize many DACs improves antenna diversity and allows for larger antenna arrays.

Performance

For the LTC2000A, Figure 2 shows the spectrum of 16 channels of CDMA with a gap channel removed. The power in each of the carriers is -36dBm and the power in the gap channel is -96dBm, showing excellent spectral purity and minimal output filtering before transmission, simplifying the setup.

Figure 3 shows a simple network used to drive the LTC2000A's output. The LTC2000A updates up to 2.7Gsps, which extends the usable bandwidth beyond 1GHz. The high sample rate also provides enough bandwidth for demanding communications applications whilst providing excellent spectral and noise performance. The LTC2000A's noise spectral density is better than 158dBc/rHz for signals up to 500MHz, which keeps the signal-to-noise ratio (SNR) high for a wide range of generated frequencies. It also has a spurious-free dynamic range better than 74dB up to 500MHz, and better than 65dB SFDR for output frequencies up to 1GHz, enabling signals to be generated without spurious content, requiring minimal filtering.

Pushing The Limits

Modern wireless designs are constantly pushing performance limits. By using multiple antennas for antenna diversity, the problem of multipath fading can easily be eliminated.

The LTC2000A makes the implementation of multiple antennas possible with its built-in synchronization features; synchronizing any number of LTC2000As can be done simply by modifying a bit in the control register. When a large number of LTC2000A devices are synchronized, they can be used in complex beamforming applications involving single or multiple antennas.

The LTC2000A can also be used with other diversity techniques such as time, frequency and code.

Electronics WORLD

Your essential electronics engineering magazine and technical how-to-guide

A subscription to Electronics World offers

- 12 monthly issues in digital format
- Regular topical supplements
- The Annual T&M Supplement
- Weekly email bulletin
- Comment and analysis from industry professionals
- Tips and tricks
- News and developments
- Product reviews
- Free invitations to our webinars

Electronics World provides technical features on the most important industry areas, including:

- Nano measurement
- Robotics, and much more...
- Power supplies
- DSPs
- Automotive
- Lighting USB design
- Signal processing
- Connectors
- Power supplies
- Semi-conductors
- Test and measurement
- Digi
- Cables
- Embedded
- Microwave
- RF
- Communica-tions

SUBSCRIBE TODAY FROM JUST £46 BY VISITING THE WEBSITE OR CALLING +44(0)1635 879 361

www.electronicsworld.co.uk/subscribe

Register for our free newsletter, please scan here

Figure 1: The proof-of-concept CXR, conjugate-matched feed demonstrator configured for corner-fed single reflector CATR geometry

Figure 2: CATR at RWTH Aachen University

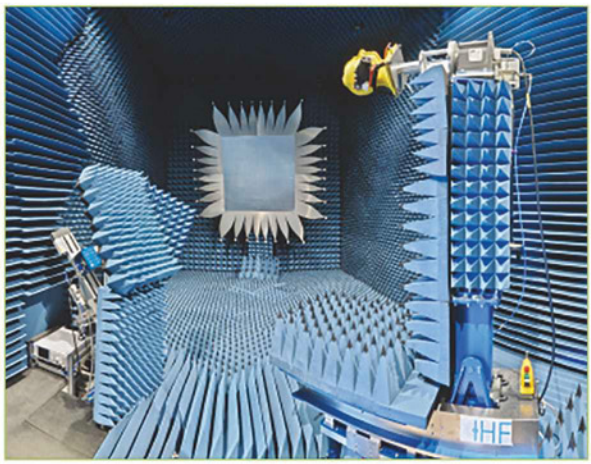

Figure 3: Field probe scanner with the Orbit/FR AL2309-AL-10.0-SL as probe (left). The CXR, conjugate-matched feed demonstrator is mounted on a feed positioner (right)

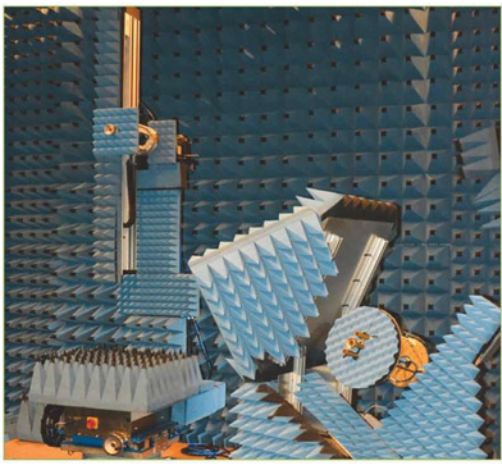

THE IMPORTANCE OF POLARIZATION PURITY

POLARIZATION PURITY OF THE ANTENNA TEST SYSTEM IMPACTS MEASUREMENT ACCURACY. **LARS JACOB FOGED**, SCIENTIFIC DIRECTOR AT MICROWAVE VISION ITALY, DESCRIBES A NOVEL FEED CONCEPT THAT EXTENDS THE MEASUREMENT CAPABILITIES OF COMPACT ANTENNA TEST SYSTEMS BEYOND TRADITIONAL LIMITATIONS

Polarization purity of an antenna system is an important characteristic, particularly in dual-polarized electronic setups, where depolarization can affect signal quality. High-calibre testing requires significantly higher polarization purity or lower cross-polarization of the test system than the test object. Compact antenna test range (CATR) systems provide convenient testing in far-field conditions of antennas placed in the test chamber's 'quiet zone' (QZ).

The CATR conveniently tests antenna systems at frequencies where far-field testing is not feasable. The CATR uses a source antenna radiating a spherical wavefront and one or more reflectors to transform the spherical wave into a planar wave within the desired test zone. In standard, single-reflector systems, a large reflector is illuminated by a feed to ensure the amplitude and phase variations are minimal across the QZ.

To avoid obstruction by the feed, it is offset, with the reflector illuminated at an angle. The offset geometry causes a variation of the polarization tilt angle as a function of position in the QZ. This geometrical optics (GO) effect gives rise to cross-polarization in the QZ.

Ensuring Accurate Testing

Accurate testing of low cross-polar antennas in CATR requires a QZ with high polarization purity. It is well known that such a condition is only achieved for testing scenarios, where the CATR reflector is at least ten times the size of the antenna under test (AUT). Unfortunately, this requirement makes accurate measurement of cross-polar performance rather difficult for larger antennas, such as arrays or reflector antennas, or antennas naturally offset in the QZ, since they are mounted on a structure, as is the case with satellite antennas.

When testing large antennas and those fitted to large platforms, the QZ cross-polar performance is often the reason why a more expensive, complex, compensated dual-reflector CATR is used rather than a single-reflector CATR. This complexity and cost deterrent is why so much research goes into minimizing the QZ cross-polarization of a single-reflector CATR. Solutions such as reflector geometry adjustments and other hardware improvements, as well as post-processing techniques, have been proposed over the years but some of the drawbacks have hindered their widespread use.

CXR Feed

The cross-polar reduction (CXR) feed is a new plug-and-play component. This novel feed concept is a breakthrough in CATR systems as it extends their measurement capabilities beyond traditional limitations and at affordable cost. The CXR feed has been conceived to significantly improve the cross-polar accuracy of side/corner-fed single reflector systems but is equally suitable for dual cylindrical reflector systems. It handles cross-polar reduction similarly to the second reflector in a dual-compensated CATR.

The CXR feed is based on an innovative architecture that works by cancelling the GO cross-polar component induced by the offset reflector; the architecture provides conjugate field matching in bandwidth of 1.5:1.

A conjugate-matched feed has aperture fields that are matched to the focal-plane fields of the reflector when illuminated by a plane wave within the QZ. Such a feed effectively cancels the GO cross-polar component, providing high QZ polarization purity in both orthogonal polarizations and unlimited bandwidth; only secondary cross-polar sources remain, such as edge diffraction effects.

Research was conducted on a conjugate-matched feed implemented as a 3-element array: a central horn which produces the co-polar illumination of the reflector, and two cross-polarized side-elements, designed to create the conjugate-field matching. In this case, the array element was optimized using a 3D full-wave simulation tool and the optimum complex array-feed excitation coefficients were determined by numerical simulation (PO/MoM) of the serrated reflector. The target minimum cross-polar discrimination of the QZ was 40dB, offering an improvement of over 10dB on classical, single-feed performance.

The physical dimensions of such a feed limit the realizable bandwidth to roughly 1.6:1 in dual simultaneous polarization and for any offset reflector configuration. In this example, the conjugate-matched feed concept was validated with a limited scope proof-of-concept CXR demonstrator, shown in Figure 1. The CXR demonstrator has been designed with a relative bandwidth of 1.25:1, covering 10GHz to 12.5GHz in single polarization.

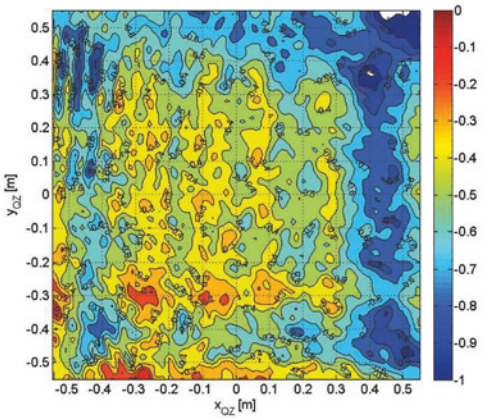

Figure 4: QZ field probing results. Contour plots of co-polarized field at 10.7GHz using traditional feed

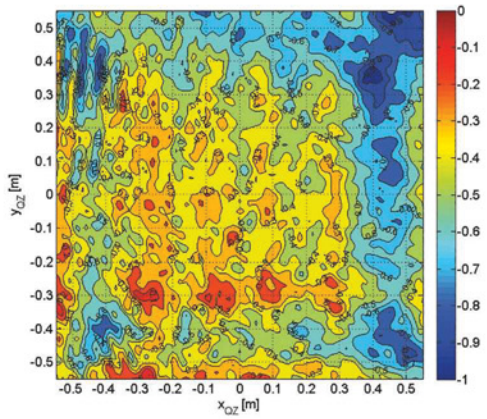

Figure 5: QZ field probing results. Contour plots of co-polarized field at 10.7GHz using the proof-of-concept CXR, conjugate-matched feed

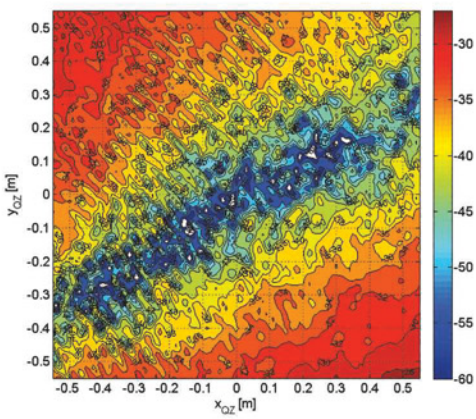

Figure 6: Contour plots of the measured QZ cross-polarization at 10.7GHz using a traditional feed

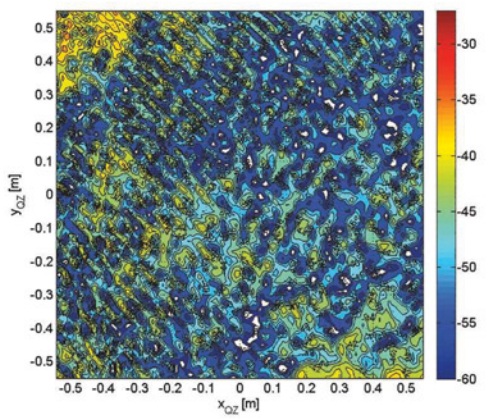

Figure 7: Contour plots of the measured QZ cross-polarization at 10.7GHz using a proof-of-concept CXR, conjugate-matched feed

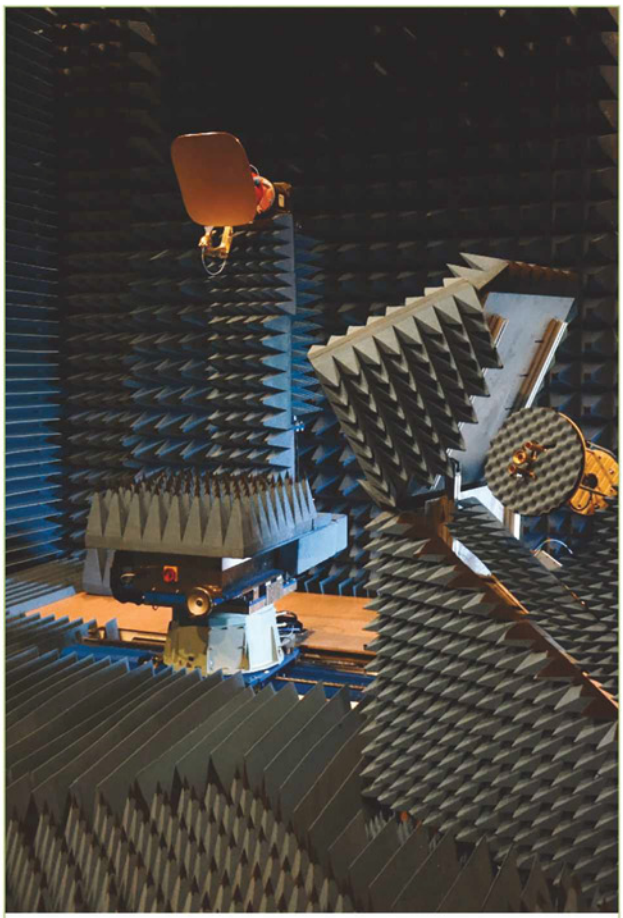

Figure 8: Reference antenna, Satimo SR40-A with SH4000 mounted on the AUT positioner (left). The CXR conjugate-matched feed demonstrator is mounted on the feed positioner (right)

Quiet Zone Probing

The CATR at RWTH Aachen University shown in Figure 2 is a typical example of a single-reflector CATR. The compact range was manufactured by MVG-Orbit/FR and is based on a corner-fed single reflector with a parabolic section of 1.7m x 1.7m and serrated edges. The resulting size of the cylindrical QZ is 1.1m x 1.1m and the operational frequency range is 2-75GHz.

The feeds are placed on a 4-axis positioner system configured as roll-over-azimuth with elevation squint and AUT pick-up, all mounted on a cross-range slide. An optimized-geometry absorber fence limits any direct leakage from the feeds to the QZ. The range is housed in a shielded chamber of 9m x 5m x 5m (L x W x H).

QZ field-probing measurements were performed using a linear field probe scanner in combination with a cross-range slide for 2D planar scanning. A standard single linearly-polarized CATR feed with medium gain and high polarization purity was used as QZ probe.

The QZ field was measured with a traditional feed and the CXR, conjugate-matched feed at the centre frequency of 10.7GHz, as shown in Figures 4 and 5 respectively. In both configurations the co-polar QZ presented appreciable co-polar field quality with maximum 1dB peak-to-peak amplitude variation, including ripple and taper effects. The field difference between the two configurations was negligible (max 0.03dB variation).

The measured cross-polar QZ field components are shown in Figures 6 and 7. The field levels have been homogenized by using the CXR, conjugate-matched feed. In particular, the worst-case cross-polarization level within the circular QZ region is reduced by more than 10dB, proving the concept of the conjugate-matched feed.

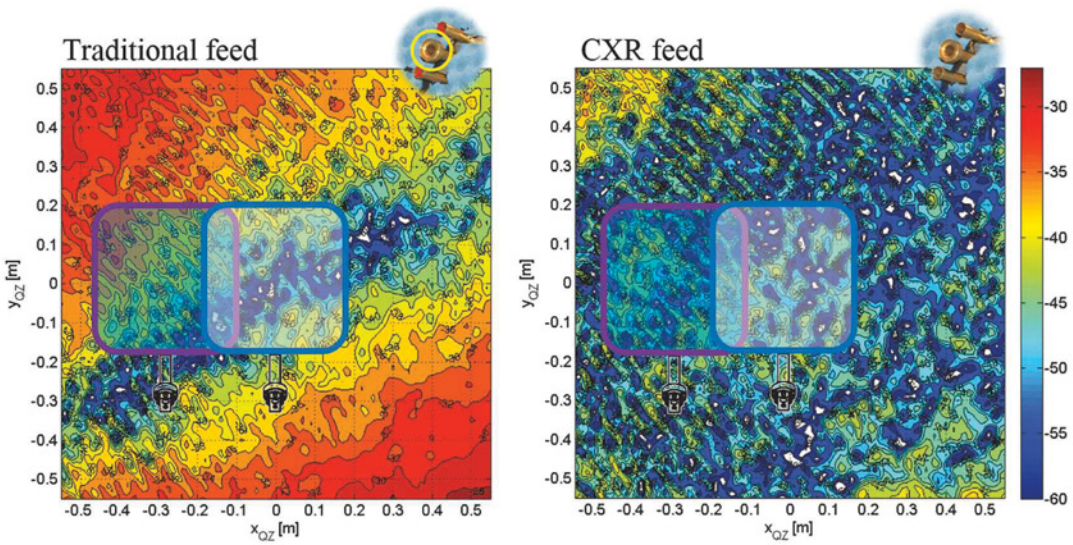

Figure 9: QZ cross-polar discrimination for centred and offset measurements of the SR-40 reflector antenna with traditional CATR feed (left) and CXR, conjugate-matched feed (right)

Space Antenna Testing Scenarios

As stated earlier, the CXR conjugate-matched feed is particularly valuable when testing electrically large antennas fitted to large platforms, such as satellite bodies.

The emulation of a space antenna testing scenario using the SR40-A reflector antenna by MVG is shown in Figure 8. The antenna is a linearly-polarized, super elliptical, offset reflector (F/D = 0.5) with a wideband dual-ridge horn feed, covering 4-40GHz. It has very low cross-polar radiation in the symmetry plane and is therefore well-suited as a demanding test object.

Test Results

In typical telecom applications, two reflector antennas are often mounted one on each side of the satellite body. In this scenario both antennas would be situated in areas of the QZ with unsatisfactory, high cross-polar levels, as shown in Figure 9. The consequence of this placement can be quantified by comparing measurements of the SR-40 reflector antenna in both the QZ centre and offset position. The measurement improvement due to the conjugate-matched feed can be determined by comparing the measurements with those of a traditional CATR feed.

> The CATR uses a source antenna radiating a spherical wavefront and one or more reflectors to transform the radiated spherical wave into a planar wave within the desired test zone

The parabolic rim of the SR-40 antenna of 400mm x 400mm is about five times smaller than the CATR reflector diameter, and sufficient to qualify the centred SR-40 measurement as reference for cross-polar performance.

As shown in Figure 10, the measured cross-polar performance of the AUT positioned at the QZ centre is very good with a cross-polar discrimination of better than 50dB. The correlation of the measured pattern is excellent when compared to the simulated reference pattern, for both configurations.

The measurement of the reference antenna in the QZ offset position is shown in Figure 11. As expected, the measured cross-polar pattern degrades by more than 10dB when using a standard feed due to the unfavourable position of the AUT in the QZ. It can be further observed that the measurement using the conjugate-matched feed is very similar to the measurement in the QZ centre position, proving that the full QZ has become available for demanding cross-polar measurements using the conjugate-matched feed.

Conjugate-Matched Feed Evolution

Although of limited scope, the conjugate-matched feed demonstrator reported in this article has successfully proven this innovative concept. The development of conjugate-matched feeds is a breakthrough for the Compact Antenna Test Ranges as it extends their measurement capabilities well beyond traditional polarization limitations at the limited cost of a new feed.

The new CXR feed is an add-on component of both side and corner-fed single-reflector CATR systems. It is equally suitable for dual cylindrical reflector systems that have similar QZ cross-polarization issues.

Based on the findings in this article, the conjugate-matched feeding concept has been further developed by MVG and implemented in the CXR feed. The final CXR feed provides simultaneous cross-polarization cancellation in both orthogonal polarizations on a full 1.5:1 bandwidth. Together, the dual-polarization and wide bandwidth of the CXR improve measurement accuracy, facilitate measurement process and shorten the overall measurement time.

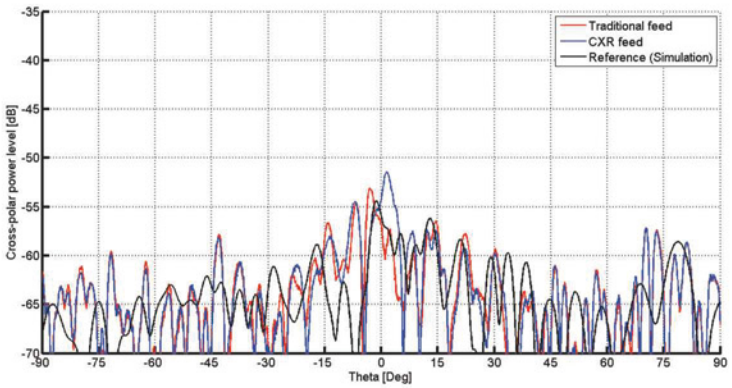

Figure 10: AUT positioned in the QZ centre. Comparison of measured and simulated cross-polarization E-plane pattern of the SR40-A at 10.7GHz. Traditional feed (red); CXR, conjugate-matched feed (blue)

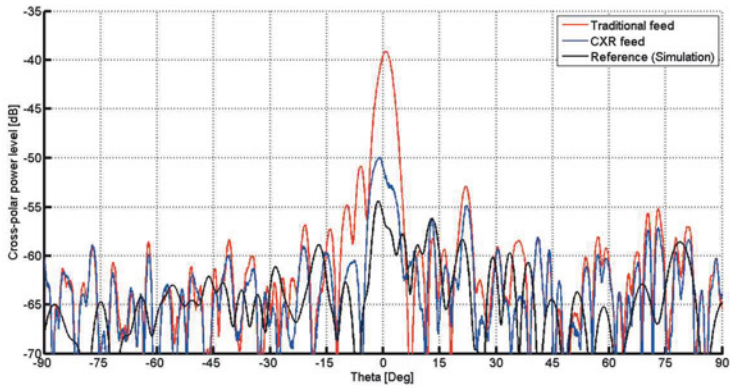

Figure 11: AUT offset -0.3m in QZ. Comparison of measured and simulated cross-polarization E-plane pattern of the SR40-A at 10.7GHz. Traditional feed (red); CXR, conjugate-matched feed (blue)

ENHANCEMENT OF WLAN ANTENNA PERFORMANCE USING AN N-LIKE SHAPE EBG STRUCTURE

M. S. ALAM, N. MISRAN, M. T. ISLAM, M. ISMAIL AND **B. YATIM** FROM NATIONAL UNIVERSITY OF MALAYSIA PRESENT A COMPACT MICROSTRIP ANTENNA FOR 5.4GHZ APPLICATIONS, WITH 235MHZ BANDWIDTH AND PEAK GAIN OF 3.9DB

Microstrip antennas are widely used in satellite communications, biomedical applications, radar, reflector feeds and other wireless communication applications. The microstrip antenna is known for its low profile, light weight, cost-effectiveness and compatibility with planar integrated circuits.

Although very popular, microstrip antennas have limitations, among them narrow bandwidth (< 5%), low gain (< 5dBi), excitation of surface waves and poor radiation performance. These shortcomings have restricted their use in many more fields.

To enhance the microstrip antenna's performance, several techniques exist in the literature, including the use of thicker substrates, stacked antenna configurations and slotted patches. However, these methods are not always suitable, and they too have limitations.

Recently, artificially-engineered electromagnetic band gap (EBG) materials have been used in microstrip antennas and were found to improve radiation performance and provide better gain and efficiency. An EBG structure/material is a periodic arrangement of metallic or dielectric patterns, which can stop the propagation of electromagnetic waves in a certain direction and within a certain frequency band.

There are different types of EBG structures, of which uni-planar ones are the most popular because of their configuration and suitability for use with microwave planar circuits. However, the design of new EBG structures is still a challenge, especially when it comes to achieving good radiation pattern, polarization and gain in the microstrip antenna.

WLAN

A wireless local area network (WLAN) is based on the IEEE 802.11a standard and provides easy access and high-speed connectivity in the 5.1-5.8GHz band. Various microstrip antenna designs have been studied and proposed for WLAN bands such as the co-planar waveguide (CPW) fed modified Sierpinksi gasket monopole, the proximity-coupled microstrip antenna, the microstrip line-fed slot antenna with rectangular tuning stubs, and the dual U-strip slot, among others; some of them are listed in Table 1.

Designing A Microstrip Patch Antenna

For some configurations, the antenna's bandwidth is sufficient but the gain needs improving. Antenna compactness is another

Ref. No.	Antenna Size (mm^3)	Bandwidth	Gain (dB)
Song et al. 2008	40 x 100 x 0.81	430 MHz (4.89-5.32)GHz, 8%/460 MHz (5.71-6.17)GHz, 7%	1.5-2.5
Thomas et al. 2011	30 x 25 x 1.57	290 MHz (5.4-5.69)GHz	4.2/5.1
Kueathaweekun et al. 2008	82 x 47 x 1.6	(2-6.35)GHz, 104%	4
Archevapanich et al. 2008	40 x 30.8 x 1.6	(4.76-6.34)GHz, 31.6%	3.4
Han et al. 2010	40 x 29.3 x 1	1.8GHz (4.9-6.7)GHz, 31%	--
Zhao and Hua 2012	15 x 12 x 1	110/370 MHz (5.17-5.28)/ (5.64-6.01)GHz	1.92/2.57
Kelothu et al. 2012	60 x 70 x 1.6	(5-6)GHz	7.1
Chitra et al. 2012	40 x 26 x 1.6	(4.736-5.432)GHz	1.5
Kim and Park 2005	20 x 15.5 x 1.6	1.92GHz (4.36–6.28)GHz, 36.1%	2.8
Danideh et al. 2009	21 x 25 x 0.5	1.35GHz (5.1-6.35)GHz, 23.8%	2.2
Chandra et al. 2010	30.5 x 46 x 1.57	8.63% (5 to 6GHz)	3.2/4
Luo et al. 2008	55 x 55 x 3	1.1GHz (4.5-5.6)GHz	2

Table 1: Performance of some recently reported 5GHz antennas

challenge since antenna size is dependent on the frequency of operation and, in turn, the antenna characteristics are sensitive to the antenna size.

Here, we present a new, ribbon-like microstrip antenna and an N-like EBG structure for improved design and performance. The EBG structure is integrated in the patch antenna to enhance its performance.

The criteria involved in the design of a patch antenna include choosing the right substrate material, patch dimension and feed position. Key parameters relating to selecting the right dielectric substrate are relative permittivity and loss tangent. The operational bandwidth of an antenna is proportional to substrate thickness, whilst it is inversely related to relative permittivity. Beside this, a higher tangent loss reduces antenna efficiency and increases feed losses.

The material chosen in this study is a 1.575mm thick Roger RT/Duroid 5880 with a dielectric constant of 2.2 and loss tangent of 0.009. Depending on the desired resonant frequency (f_0), which is 5.4GHz, the thickness (h) and dielectric constant (ε_r) of the substrate, and length (L) and width (W) of the patch antenna can be determined by using the following equations:

$$W = \frac{c}{2f_o}\left(\frac{\varepsilon_r + 1}{2}\right)^{-\frac{1}{2}} \quad (1)$$

$$\varepsilon_e = \frac{\varepsilon_r + 1}{2} + \frac{\varepsilon_r - 1}{2}\left[1 + \frac{12h}{W}\right]^{-\frac{1}{2}} \quad (2)$$

$$L = \frac{c}{2f_r\sqrt{\varepsilon_e}} - 2\Delta L \quad (3)$$

$$\Delta L = 0.412h\frac{(\varepsilon_e + 0.3)\left(\frac{W}{h} + 0.264\right)}{(\varepsilon_e - 0.258)\left(\frac{W}{h} + 0.8\right)} \quad (4)$$

where the patch ΔL is the additional length needed on the antenna's end due to a fringing field along its width, ε_e is the effective dielectric constant and c is the speed of light in a vacuum.

We calculated the 5.4GHz rectangular patch to be 22 x 18mm². However, we modified the microstrip antenna design into a ribbon-like shape, reducing its size, and added an L-slot onto it, whilst maintaining the resonant frequency of 5.4GHz.

The optimized dimensions of the proposed antenna are now L = 14.58mm and W = 15.86mm. The antenna's excitation is by a coaxial-probe feeding method, as shown in Figure 1. Figure 2 shows the return loss characteristics for different patch shapes.

Several other studies have been carried out on the design parameters, like feeding probe position, L-slot length in x and y directions and so on, to examine the performance of a microstrip patch antenna relating to its resonant frequency, bandwidth and gain.

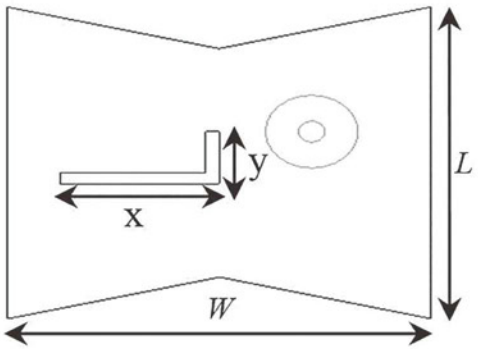

Figure 1: Ribbon-like shape of a microstrip patch antenna

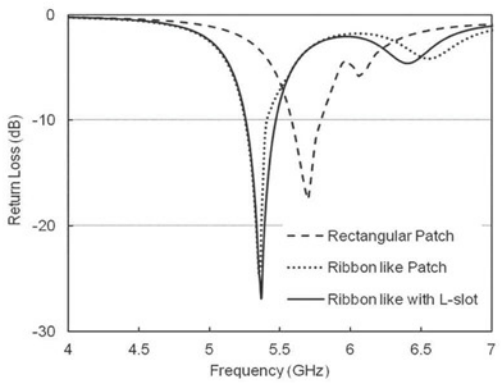

Figure 2: Return loss characteristics for different patch shapes

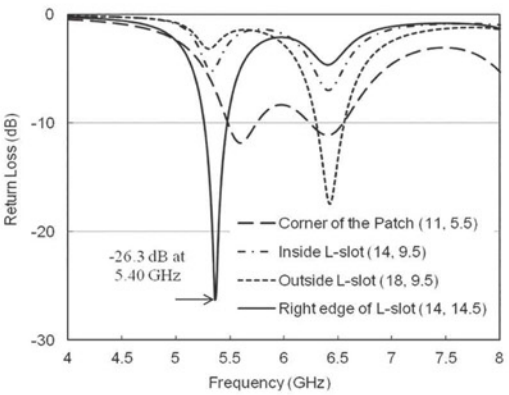

Figure 3: The effect of different probe feed positions on return loss

Feeding Probe Position

The feeding position is an important issue in designing a microstrip patch antenna, since it affects impedance matching and hence the desired resonance. Figure 3 shows the return loss graph obtained from four different feed positions. By varying the excitation positions (all around the L slot), different return loss

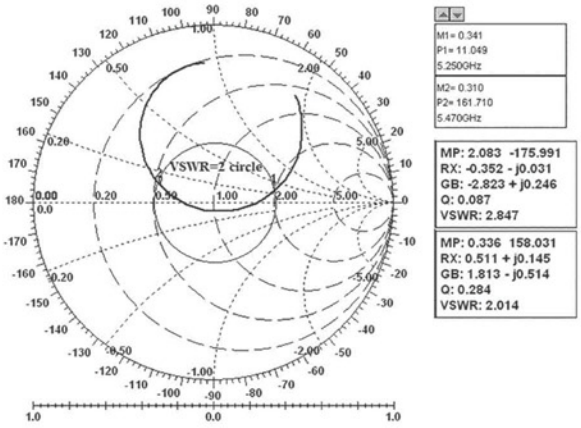

Figure 4: Smith chart for the ribbon-like patch antenna

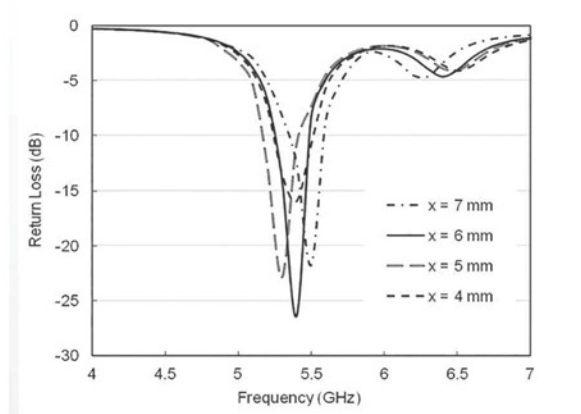

Figure 5: Effects of L-slot length x on return loss

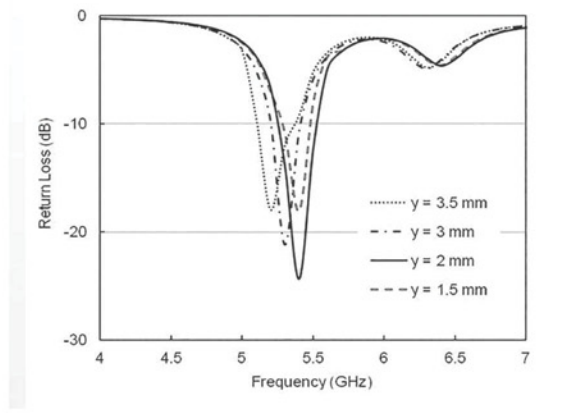

Figure 6: Effects of the L-slot length y on return loss

curves are obtained, and in some cases no resonance occurs.

The best position found is at (14, 14.5) coordinates, just on the right edge of the L slot (as shown in Figure 1), where the minimum return loss is -26.3dB at 5.4GHz.

The Smith chart shown in Figure 4 helps determine the impedance matching and bandwidth; it can be seen that the operational bandwidth is 5.25-5.47GHz with VSWR ≤ 2.

L-Slot Dimensions

With the selected best feeding position, the patch is excited with different lengths x of the L-slot, which is varied from 4-7mm; the respective return losses are shown in Figure 5. It can be seen that, although the return loss curves do not change very much, the bandwidth is wider and there's a good return loss level. Table 2 shows the values when the slot's length x is varied.

The effect of another L-slot length y variation were also analyzed; the results are shown in Figure 6 and summarized in Table 3. The bandwidths are almost similar but the resonant frequency has shifted with the length variation. The peak gain changes from 3.9 to 4.1dB for different values of y.

Furthermore, the effects of L-slot width (Ws) on the antenna return losses were analyzed. We note that the upper frequency limit changes but not so the lower limit. However, compared to others, the 0.5mm-wide slot provided a deep return loss with a wide bandwidth. Table 4 shows antenna performances for various W_s.

EBG Structure

We designed an EBG structure that consists of an N-like unit cell (shown in Figure 7), which has been applied to the ribbon-like antenna. This unit is 10mm x 10mm in size, with two symmetrical triangular slots. Each unit is connected to four adjacent cells through four 4mm x 0.2mm connecting bridges. Unlike the conventional mushroom-like EBG which has vias connected to ground, the proposed EBG structure is completely vialess, where all EBG unit cells interconnect through a narrow strip. Theoretically, the period of the EBG structure has to be smaller than λ/2 at the resonant frequency, which is 28mm at 5.4GHz. However, by introducing two symmetrical triangular slots and narrow strip bridges, the periodicity P of the proposed N-like EBG structure is reduced to only 12mm, thus reducing the required antenna size by 57%.

The bandgap characteristics of the structure are determined by the suspended microstrip line method. The transmission responses (S21) for various sets of triangular slot dimensions (denoted by p, q and r) are shown in Figure 8. It can be seen that the bandgap frequency has shifted to a higher frequency range, which doesn't cover the desired resonant frequency; whereas the bandgap achieved for the proposed EBG structure (3.8, 3 and 4.8mm) has a frequency range of 5.12-6.72GHz (1.6GHz) at -20dB of transmission coefficient S21. The slot size has been adjusted to obtain a bandgap covering the antenna's operating bandwidth.

After determining the bandgap behaviour, the EBG structure is incorporated with the ribbon-like patch, sandwiched between two similar dielectric substrates (ε_r = 2.2 and h = 1.575mm). The

Length x (mm)	Return loss (dB)	Resonant Frequency (GHz)	Bandwidth (GHz)	Gain (dB)
7	-21.51	5.50	5.44-5.53	3.71
6	-26.37	5.40	5.24-5.48	3.85
5	-22.84	5.30	5.16-5.45	3.78
4	-15.96	5.35	5.25-5.47	3.83

Table 2: Effects of slot length x on antenna performance

Length y (mm)	Return loss (dB)	Resonant Frequency (GHz)	Bandwidth (GHz)	Gain (dB)
3.5	-17.94	5.23	5.18-5.38	3.9
3	-21.15	5.33	5.22-5.41	4.1
2	-26.37	5.40	5.24-5.48	3.85
1.5	-18.04	5.38	5.27-5.42	3.97

Table 3: Effects of slot length y on antenna performance

Slot width (W_s)	Return loss (dB)	Resonant Frequency (GHz)	Bandwidth (GHz)	Gain (dB)
0.7	-16.51	5.33	5.24-5.41	3.61
0.65	-18.04	5.31	5.22-5.43	3.84
0.55	-18.16	5.35	5.23-5.46	3.76
0.5	-26.37	5.40	5.24-5.48	3.85

Table 4: Effects of L-slot width (W_s) variation

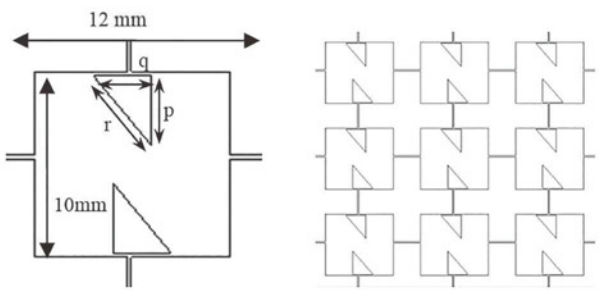

Figure 7: N-shape EBG unit (left); 3x3 EBG structure (right)

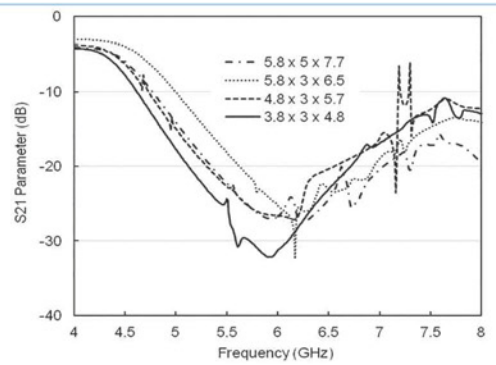

Figure 8: Effects of triangular slot dimensions on the S21 parameter

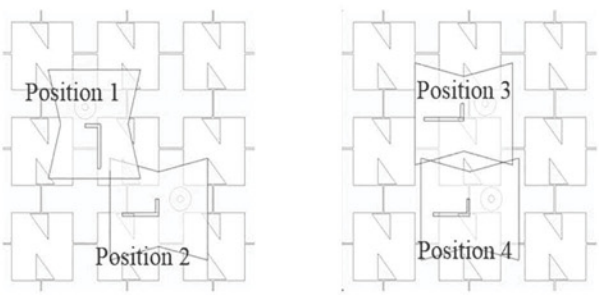

Figure 9: Patch antenna orientation on the EBG structure

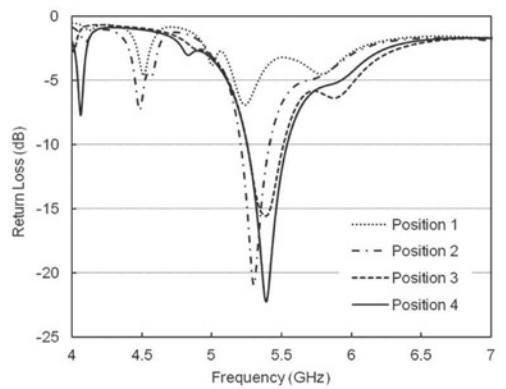

Figure 10: Respective return losses for various patch positions

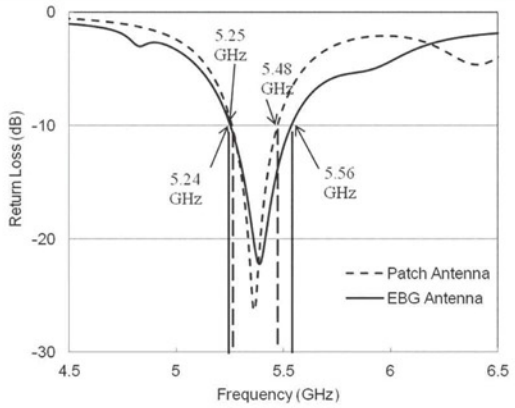

Figure 11: Return loss (S11 parameter) comparison of the proposed antenna with and without the N-shape EBG structure

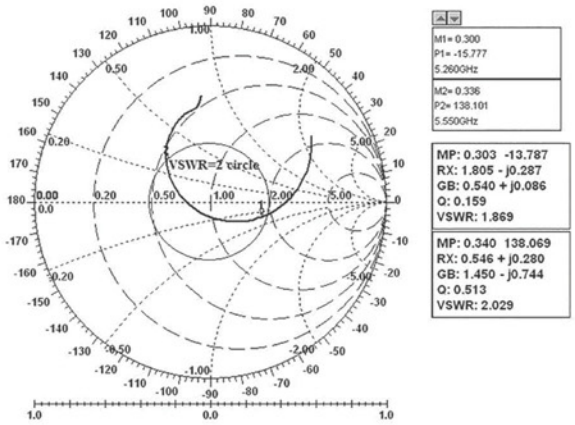

Figure 12: Smith chart for the patch antenna with EBG structures

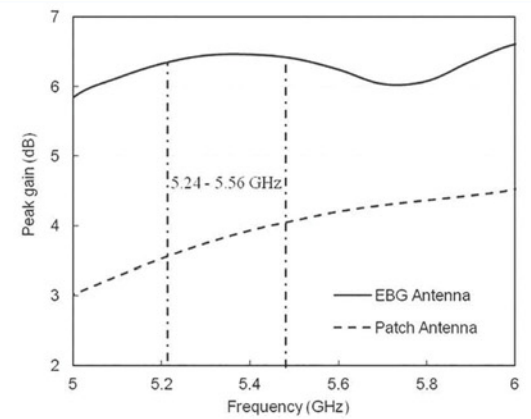

Figure 13: Peak gain of the antenna with and without the EBG structure

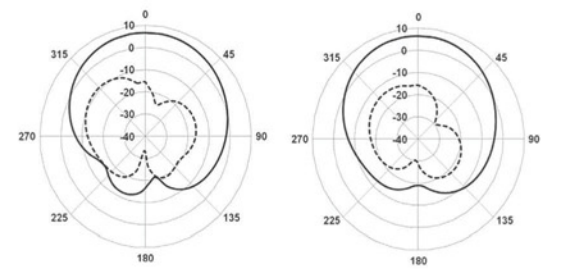

Figure 14: E-plane (left) and H-plane radiation patterns of the EBG microstrip antenna at 5.4GHz; solid line: Co-pol; dashed line: Cross-pol (right)

Antenna without EBG	Antenna with EBG
5.25-5.48GHz (4.26%)	5.24-5.56GHz (5.93%)
-26.37dB	-21.69dB
3.61-4.05dBi	6.42-6.58dBi

Table 5: The proposed antenna with and without the EBG structure

antenna is mounted on the top layer and the orientation of the patch is adjusted for best possible performance.

Figure 9 shows the patch orientations on the EBG structure and Figure 10 shows the respective return loss behaviour. Position 1 of the patch gives the worst behaviour, whilst the best result is found at position 4. The resonance shifts lower when in position 2, whereas the minimum return loss for position 3 (-15.5dB) is not as deep as with position 4 (-21.69dB) at the resonant frequency of 5.4GHz.

Figure 11 compares return loss characteristics for the antenna with and without the EBG structure. The EBG antenna has a bandwidth increment of 90MHz, covering the range 5.24-5.56GHz. Although the return loss level increases slightly, the improvement is quite remarkable. The Smith chart shown in Figure 12 for the proposed EBG antenna shows the impedance matching within the bandwidth.

Peak gain curves of both antennas (with and without EBG) are compared in Figure 13. Over the operating band, the gain is improved by the EBG and is stable throughout the bandwidth. Maximum gain obtained at 5.4GHz is 6.5dB for the EBG case, 2.58dB higher than that of the antenna without EBG (3.92dB). Peak gain is 1.04dB higher for the final design. Patch orientation and position were important factors in achieving this, higher, gain.

Radiation characteristics of the antenna are shown in Figure 14. In both E and H planes, the co-polarization level is distinctly higher than the cross-polarization level, always desirable for better performance. Since the EBG structure suppresses the unwanted surface waves and reduces back-radiation, the gain is enhanced and directivity increased. The recommended antenna characteristics are shown in Table 5.

SOUTHERN 15 Manufacturing & Electronics

FIVE | Farnborough | Hants | GU14 6XL

9th to 11th February 2016

A World Of Electronics At Southern Electronics 2016

Southern Manufacturing and Electronics returns to FIVE, Farnborough, from February 9th to 11th, 2016. The show continues in its popular three-day format, making it easier to plan a trip to the UK's largest and longest-running electronics exhibition.

Keeping up to date with the latest innovations in components and sub-assemblies is no easy task, but with its extensive range of suppliers in a single venue, Southern Electronics makes that job considerably easier. The proof is also in the show breaking attendance records on a yearly basis for over a decade, now considered by many the Number One electronics event in the UK.

Easy Location

Situated close to the M3 in Hampshire and well-served by public transport, the event is easily accessible, and offers free entry and free on-site car parking. The three-day opening introduced last year allows visitors more flexibility in scheduling their visits, as well as helps attract exhibitors from an ever-wider geographic area, which now includes the whole of Europe from Lithuania and Estonia to Spain and Italy.

Southern Electronics's combination of design, production and components gives the event a unique profile and atmosphere. Some 50% of the 18,000m² exhibition area is dedicated to electronics, attracting visitors from every branch of the industry.

Within the manufacturing areas, visitors will find an equally vast range of vendors providing everything from state-of-the-art machine tools and automation systems to nylon stand-offs and fixings. Engineering services range from design to box-build, and precision engineering to heavy fabrication. There're are several hundred production equipment suppliers showing their products and services, from advanced stock management systems, optical inspection and soldering to complete clean room solutions, and even anti-static flooring and industrial lighting.

Vast Range Of Exhibitors

Among its range of exhibitors are major international suppliers such as RS Components, Cosel Europe, Yamaichi Electronics, Hirose, Lemo, Molex, Midas Components, Nexus GB, Sinclair Rush and many more, to much more specialised suppliers and service providers, such as York EMC, METECC, SIC, Gem Cable and Bytesnap Design, giving visitors an opportunity to see highly-skilled companies.

The event is also the pre-eminent marketplace for subcontracting and specialist engineering services of all types. The European PCB industry is represented by firms such as Espirit Circuits, Eurocircuits, PCB Baltic and European Circuits. Firms like Blundell Production Equipment, Optris and Bondline Electronics provide production hardware, while companies such as Easby Electronics, JJS Manufacturing, CT Production, ERNI Electronics and EC Electronics showcase different types of design and build services.

Within the Manufacturing area, visitors will meet a thorough cross-section of the UK's top precision engineering firms. Other areas of advanced manufacturing will include composites, engineering plastics and additive manufacturing. Technology Trails will guide attendees around the exhibition, enabling them to best organize their time at the show. Sectors covered include aerospace, automotive, contract electronics manufacturing and medical technology.

Other specialist areas, for example the live demonstration Machinery Centre, will enable visitors easily locate products and services. A tiny selection of the offerings highlighted in 2016 will include CNC machine tools and machining centres, CAD/CAM tools, advanced adhesives, fasteners and joining technology, 3D printing, laser cutting, packaging solutions, labelling and marking, pressings, fabrications and enclosures, metrology and test equipment, coating and finishing, motors, drives and controls and handling and storage.

Seminars

Combined with the exhibition and demonstration areas, Southern Electronic's free seminar programme is a hugely popular draw for show attendees. Two programmes run in tandem in two theatres, focusing on engineering and electronics respectively, covering discussions on technical breakthroughs, business management, design and current commercial regulation. Access to these high-calibre engineering and business expertise is free.

The full list of seminars and the all-important pre-registration, can be seen at www.industrysouth.co.uk.

Although admission to the show is free for business visitors, registration is necessary. To register for tickets, visit www.industrysouth.co.uk.

Show visitors can keep up to date with the latest event and exhibitor news by visiting the show's official blog, http://blog.industrysouth.co.uk, by following @industry_co_uk #southmanf on Twitter or by joining the show's official group on the popular business networking site LinkedIn at http://linkedin.industrysouth.co.uk.

For more information call Phil Valentine on +44 (0)1784 880890, fax +44(0) 1784 880892, email philv@etes.co.uk or go to ***www.industrysouth.co.uk***

ANALYZING THE ELECTRICAL PERFORMANCE OF LARGE REFLECTOR MESH-SURFACE ANTENNAS

CONGSI WANG, **MINGKUI KANG**, **WEI WANG**, **MENG WANG** AND **JING MAO** FROM XIDIAN UNIVERSITY IN CHINA PROVIDE THEORETICAL GUIDANCE FOR THE ANALYSIS OF MESH-REFLECTOR ANTENNA PERFORMANCE

Since the 1960s, the space antenna has found a wide application range, including in satellite communications, remote sensing measurement, deep-space exploration and military reconnaissance. NASA was the first to carry out systematic studies on the design and applications of the mesh antenna, followed by research in other countries. The US and Russia have had a technical advantage in the R&D of the reflecting mesh, a special design that reflects radio frequencies. Their mesh is characterized by high elasticity, great thinness and light weight.

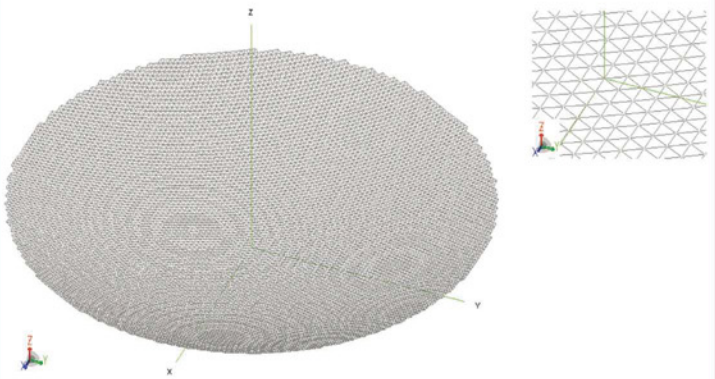

Figure 1: Mesh (triangular) reflector model and local magnification

Reflecting Mesh

The reflecting mesh is woven in a very complicated way, which has been simplified in the literature into a round conductor rule. Unlike a solid surface, many parameters of the mesh surface, such as mesh size, energy leakage and contact between the metal wires, influence the antenna's electrical performance, making it more difficult to analyze. Therefore, at the early stages of the antenna design, it is necessary to model the reflecting mesh and to determine its electrical performance, which will help reduce antenna cost and shorten the overall design phase.

FEKO (FEldberechnung bei Körpern mit beliebiger Oberfläche) is electromagnetic analysis software widely used in antenna design, configuration and EMC analysis. However, one of its disadvantages is that the antenna's line element can only be analyzed by the method of moments (MoM) modeling, using specialized software to predict the patterns of arrays.

When the reflector's aperture is large but the mesh hole is small, a great number of nodes and their connections must be considered in the modeling, resulting in a large coefficient matrix. Such a large matrix should be stored and inversely calculated, which is beyond the capabilities of a computer, making the analysis impossible. For example, if the diameter of the antenna is 1m, its focus length 0.667m, and the mesh hole is a triangle with 1mm element length, the model contains 2,718,162 line elements, more than can be analyzed with a PC. As such, practical limitations on computing time and computation power greatly restrict analysis of antenna

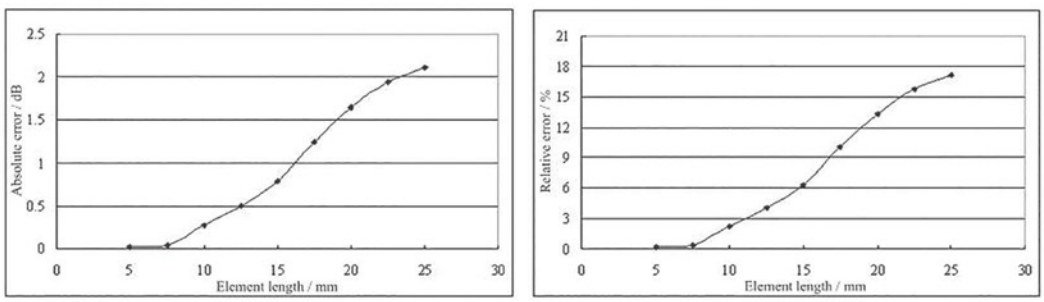

Figure 2: Change of absolute gain error and relative gain error with varied element lengths

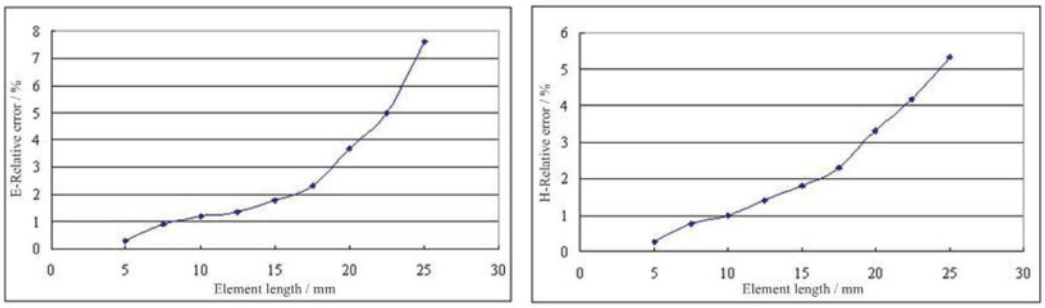

Figure 3: Change of relative error of sidelobe level on the E and H planes with varied element lengths

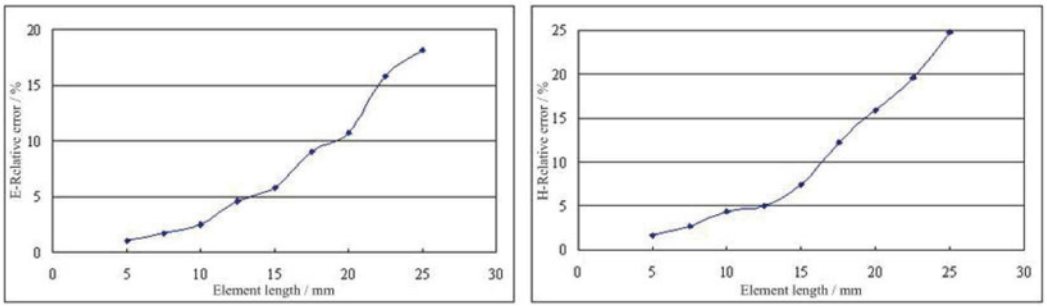

Figure 4: Change of relative error of half power-beamwidth on the E and H planes with varied element lengths

performance; optimizing the available resources to complete it becomes essential.

In view of that, we carried out this study on the equivalent analysis of the mesh structure of a large paraboloid antenna.

Modeling And Analysis

Because the mesh in FEKO comprises a large number of line elements, we first use C/C++ or Matlab to generate the line elements' endpoint coordinates and determine the corresponding connections. Then, we write the information into model file *.dat, according to the FEKO data format. A quarter of the model can be established by introducing the file into FEKO; the whole model is created by mirroring and replication.

For the analysis we used MoM to analyze the mesh, and the physical optics method to analyze the solid surface. By comparing these results with those from the electrical performance analysis, we determined the equivalent conditions in which the mesh can be treated as a solid surface; the parameters are:

Aperture	**500mm**
Ratio of focal length to diameter	**2/3**
Feed source	**half-wave dipole (2GHz) at focus and polarized along axis X**
CPU/Memory	**Intel(R) Core2 Quad Q8200 2.33GHz/8G**
Analysis software	**64bit FEKO5.4 with parallel processing on**
Mesh element length	**5, 7.5, 10, 12.5, 15, 17.5, 20, 22.5, 25 (mm)**

Triangular Mesh

Figures 2-4 show that when the element length $l \leq 0.08\lambda$, the absolute gain errors of the mesh and solid surfaces are less than 0.5dB (when l =12.5mm, the absolute error is 0.4977dB), in which case they can be considered as the same. Meanwhile, the relative errors of the sidelobe level and half of the power-beamwidth on the E/H planes are both less than 5%. Therefore, it can be assumed that with a triangular mesh and $l \leq 0.08\lambda$ the mesh surface can be treated as solid.

Tables 1 and 2 list the electrical performance parameters and necessary computing data of a solid surface and a surface of triangle meshes with element lengths of 5mm. It is known that when the mesh surface is treated as a solid surface, the accuracy reduces a bit but computing time and computation space are greatly conserved, allowing the data analysis to be performed on a common computer.

Square Mesh

Figures 5-7 show that when $l \leq 0.05\lambda$, absolute gain errors of the mesh and solid surfaces are both less than 0.5dB (when l = 7.5mm, the absolute error is 0.3067dB). In this case, the relative errors of the sidelobe level and of half power-beamwidth in the E and H planes are both less than 5%. Therefore, if the mesh is square and $l \leq 0.05\lambda$, the mesh surface can be treated as solid.

Tables 3 and 4 show the electrical performance parameters and necessary computing data for a solid surface and square meshes made up of 5mm element lengths, respectively.

Comparison between Tables 1 and 3 shows that when the mesh changes from square to triangular, the number of units

MODEL TYPE	GAIN	SLL	HPBW	TIME	MEMORY
Mesh (5mm)	12.3214dB	-9.6588dB	17.7514°	19047.61s	1016.914M
Solid Surface	12.3378dB	-9.6874dB	17.5620°	0.656s	0.795M
Absolute Error	0.0164	0.0286	0.1894	——	——
Relative Error (%)	0.1329	0.2952	1.0784	——	——

Table 1: Comparison of electrical performance parameters on the E plane

MODEL TYPE	GAIN	SLL	HPBW	TIME	MEMORY
Mesh (5mm)	12.3214dB	-6.8847dB	16.7018°	19047.61s	1016.914M
Solid Surface	12.3378dB	-6.9026dB	16.4367°	0.656s	0.795M
Absolute Error	0.0536	0.0179	0.2651	——	——
Relative Error (%)	0.1329	0.2593	1.6128	——	——

Table 2: Comparison of electrical performance parameters on the H plane

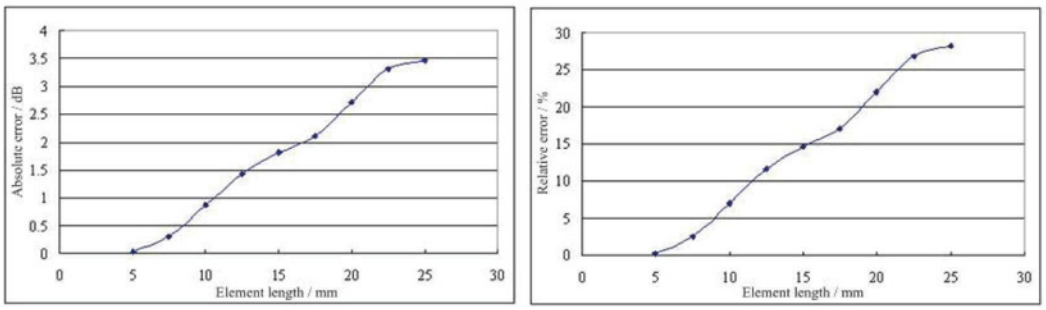

Figure 5: Change of absolute gain error and relative gain error with element length

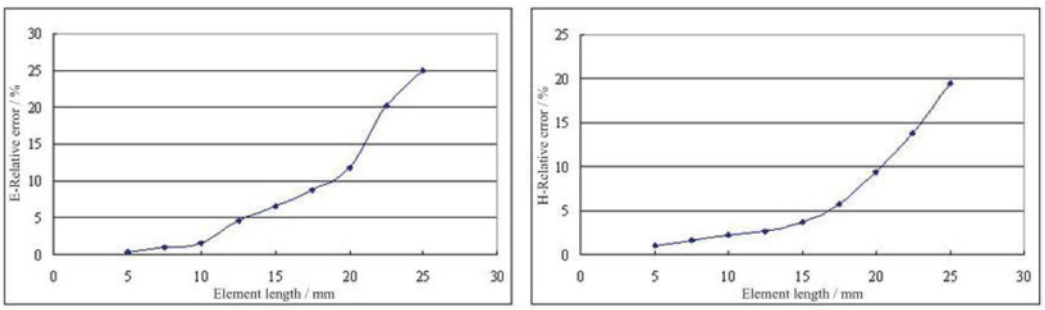

Figure 6: Change of relative error of sidelobe level on the E and H planes with element length

increases from 15,855 to 26,833, computing time increases from 1943.782s to 19047.61s, and the computation space required increases from 211.14M to 1016.914M. If the aperture of the reflector continues to increase or the unit mesh length decreases, the total line elements in the mesh model and necessary computing data will sharply and greatly increase, beyond the capabilities of a PC.

Analysis shows that with a square mesh and $l \leq 0.05\lambda$ or a triangular mesh and $l \leq 0.08\lambda$, the mesh reflector can be treated as a solid reflector, and the electrical performances in the two cases are almost the same. Therefore, in modeling, the mesh can be neglected, the node coordinates of the upper chain can be read directly, and a large number of triangular planes can be used to approximate the reflector. That way computational accuracy is guaranteed, whilst computing time and computation space are greatly reduced, achieving smooth analysis of the electrical performance of a large mesh reflector antenna.

By analyzing two different mesh shapes, we found that the triangular mesh has a larger effective reflecting area, closest of the two to a solid reflector.

This model can also show the effect of thermal deformation on antenna performance resulting from space radiation. This helps tremendously the analysis of performance of the distorted model, as it can truly reflect real working conditions, providing more accurate reference and information for mesh surface adjustment. ●

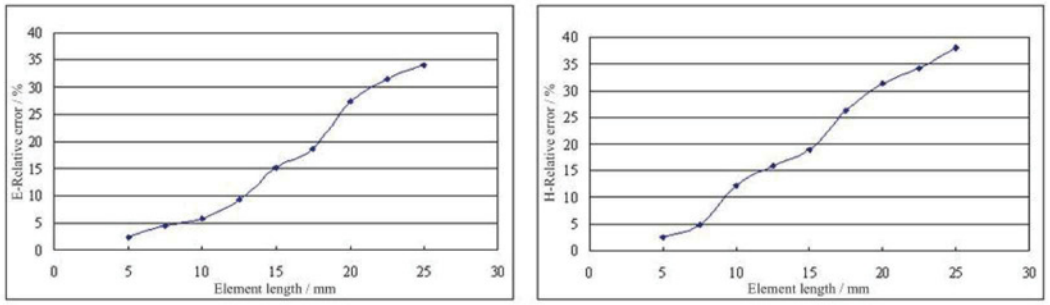

Figure 7: Change of relative error of half power-beamwidth on the E and H planes with varied element lengths

MODEL TYPE	GAIN	SLL	HPBW	TIME	MEMORY
Mesh (5mm)	12.3036dB	-9.6369dB	17.9256°	1943.782s	211.140M
Solid Surface	12.3378dB	-9.6874dB	17.5620°	0.656s	0.795M
Absolute Error	0.0342	0.0505	0.3636	——	——
Relative Error (%)	0.2772	0.5213	2.0703	——	——

Table 3: Comparison of the electrical performance parameters between two models on the E plane

MODEL TYPE	GAIN	SLL	HPBW	TIME	MEMORY
Mesh (5mm)	12.3036dB	-6.8656dB	16.8502°	1943.782s	211.140M
Solid Surface	12.3378dB	-6.9026dB	16.4367°	0.656s	0.795M
Absolute Error	0.0342	0.0370	0.4135	——	——
Relative Error (%)	0.2772	0.536	2.5155	——	——

Table 4: Comparison of electrical performance parameters between two models on the H plane

HIGH-GAIN METAMATERIAL FOR SATELLITE ANTENNA APPLICATIONS

BY **M. I. HOSSAIN, M. R. I. FARUQUE** AND **M. T. ISLAM,** NATIONAL UNIVERSITY OF MALAYSIA, WHO ALSO PROPOSE A MICROSTRIP PATCH ANTENNA SUITABLE FOR X-BAND COMMUNICATIONS

Low-profile and high-performance antennas are in greater demand for all types of communications. The microstrip patch antenna is widely used, since it offers a low profile, compact design, light weight, it's easy to manufacture and is low in cost. However, among its drawbacks are narrow bandwidth, low gain and poor polarization.

To overcome some of these issues, various techniques are applied, including using thin substrates (for better conductivity), different feed- and impedance-matching techniques, and different structures. For example, a wide-slot microstrip antenna with a fork-like tuning stub offers wider bandwidth; and slotted microstrip antennas printed on FR4 substrates also show improved bandwidth and gain (about 2dBi).

> The proposed metamaterial array configuration leads to slightly shifted resonance points compared to that of the unit-cell

X-Band Communications

The X-band covers the 8-12GHz range, and is widely adopted in many applications because of its high transmission rates, large bandwidth and short-range features, which are deemed highly suitable for satellite communications applications.

A microstrip patch antenna is suitable for X-band applications, however it can suffer from insufficient gain. A sectoral patch antenna with rectangular and circular slots on the ground plane and a radiating patch can help, but we chose a different approach, by creating a new metamaterial embedded microstrip patch antenna. We used a planar, one-layer, double negative metamaterial array as the superstrate for the antenna to improve its gain. We then analyzed the antenna performance, with and without the metamaterial, to establish its effects.

Figure 1a shows the geometry of the proposed microstrip antenna, which consists of a rectangular patch, partial ground plane and printed microstrip line. The feed line is situated between the microstrip and ground, and uses an SMA connector of 50-ohm normalized impedance. We used a 0.8mm FR-4 sheet as substrate.

We fabricated a prototype of the antenna using printed circuit techniques as shown in Figure 1b. The antenna dimensions are 40mm × 40mm × 0.8mm. We used computer simulation technology for its design, and measuring its performance in an anechoic chamber. We used a vector network analyzer (Agilent N5227A) to observe the antenna's reflection coefficient. Figure 1c shows the surface current distribution of the proposed antenna at 11.3GHz.

Metamaterial Design

Figure 2a shows the structure of the metamaterial unit-cell and array. The array is also fabricated on a 0.8mm FR-4 substrate using printed copper strips.

The metamaterial unit-cell consists of two circular split resonator structures. The radii of the inner and outer rings are

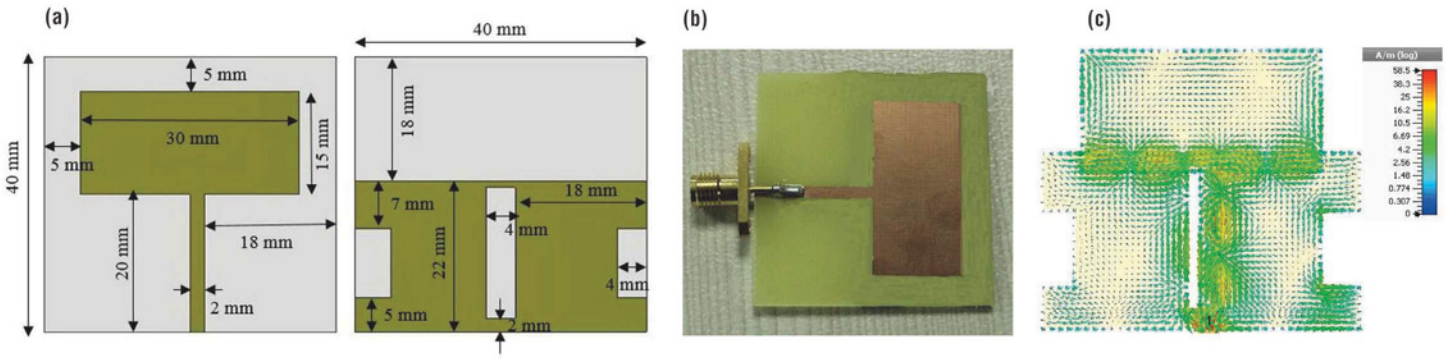

Figure 1: (a) Proposed antenna geometry; (b) fabricated prototype of the antenna; (c) surface current distribution of the proposed antenna at 11.3GHz

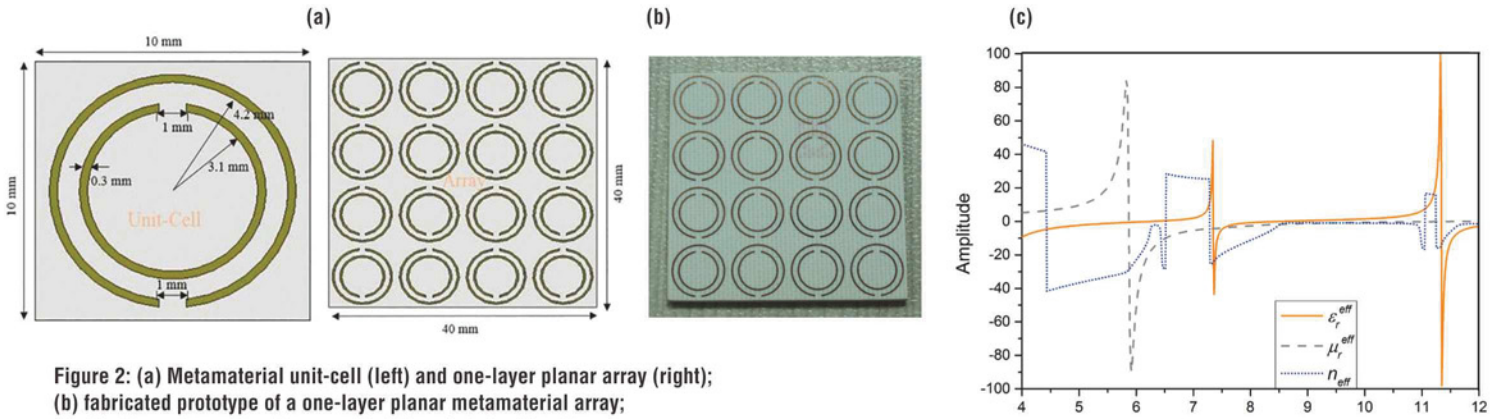

Figure 2: (a) Metamaterial unit-cell (left) and one-layer planar array (right); (b) fabricated prototype of a one-layer planar metamaterial array; (c) effective parameters of proposed metamaterial unit-cell

3.1mm and 4.2mm respectively, with a 0.3mm-wide circular strip and 1mm split gaps. The dimensions of the metamaterial unit-cell are 10mm × 10mm × 0.8mm.

A 40mm × 40mm × 0.8mm large, planar, one-layer metamaterial array is formed using only 4 × 4 unit-cells. The dimensions of the metamaterial unit-cell and array are chosen to get double-negative characteristics at the operating frequencies of the proposed antenna.

The effective parameters of the metamaterial unit-cell (permittivity and permeability) are determined from the scattering parameters (S11 and S21) using the Nicolson Rose Weir (NRW) method. Figure 2c shows the effective permittivity, effective permeability and effective refractive index of this unit cell between 4GHz and 12GHz. The results successfully prove that the unit cell acts as a double-negative metamaterial from 11-12GHz. The figure also shows negative permeability from 6GHz to the end of the frequency range.

In the antenna's operating band, the proposed metamaterial also exhibits negative refractive index in the range 11.2-12GHz. This array configuration leads to slightly shifted resonance points compared to the unit cell, and the simultaneous negative values of the effective permittivity and permeability are still observed from these points over the antenna's full operating range.

Figure 3a shows that the metamaterial superstrate is 10mm away from the antenna radiator. The front side of metamaterial planar layer (printed copper structure) is placed opposite the antenna patch. Plastic support is used between the antenna and superstrate.

Figure 3b shows the reflection coefficients for the antenna with and without the metamaterial superstrate. It can be seen that the metamaterial superstrate layers affect the antenna's resonance points. The optimal distance between the antenna and superstrate is shown to be 10mm, based on the fact that the antenna's bandwidth does not decrease when using a superstrate. If the distance between the antenna and metamaterial superstrate is less than 10mm, then the antenna impedance mismatch becomes higher and the bandwidth reduces. Moreover, the proposed metamaterial antenna has a wide impedance bandwidth from 10-12GHz (2GHz) using a -10dB reference.

Figure 3c shows the values of the antenna's radiation efficiency with and without metamaterial superstrate configurations, confirming that the metamaterial substrate does not significantly affect radiation efficiency.

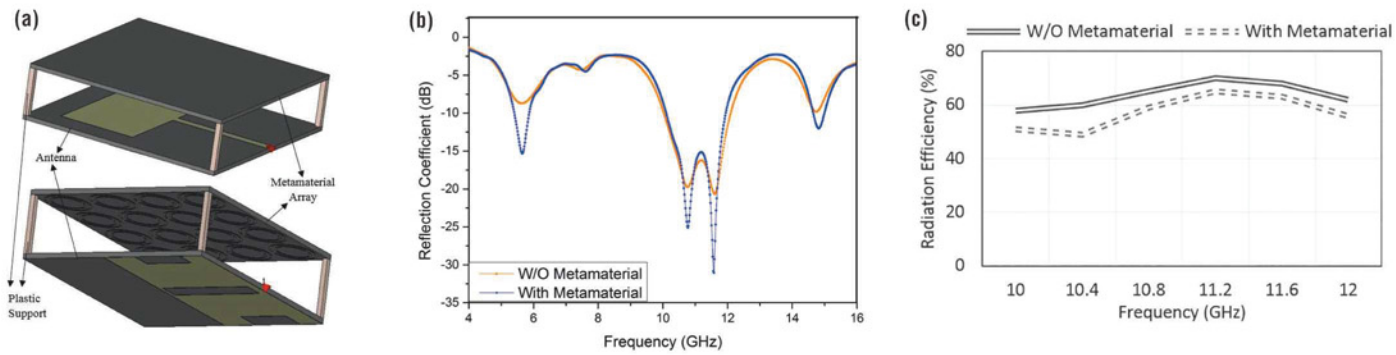

Figure 3: (a) Antenna with three metamaterial layer; superstrate configurations; (b) reflection coefficients of antenna with and without metamaterial substrate; (c) radiation efficiencies of the proposed antenna with and without metamaterial superstrate

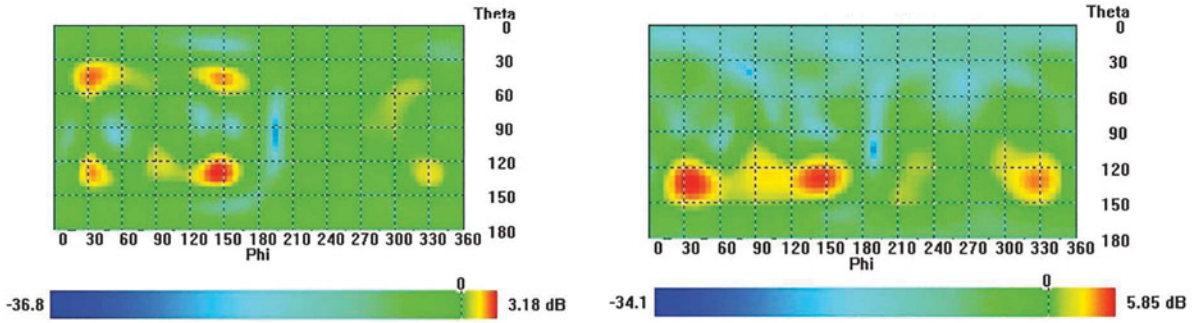

Figure 4: 2D radiation pattern of the antenna: (a) without a metamaterial layer; (b) with metamaterial layer

The radiation efficiency of the proposed antenna varies from 52-70%, with highest efficiency exhibited at 11.2GHz. Results also show that the antenna gain is dramatically increased thanks to the double-negative metamaterial layer.

Antenna gains with and without metamaterial superstrate are 5.85dBi and 3.18dBi respectively at 11.3GHz. So, using a one-layer planar metamaterial array leads to a 2.67dBi improvement in gain.

Figures 4a and 4b show the 2D radiation patterns of the antenna with and without the metamaterial superstrate when both phi and theta angles at 11.3GHz are varied. The gain is also shown in these figures using colour variations.

DESIGN OF A MIMO-MB UWB SYSTEM FOR MULTIPLE MODULATION SCHEMES

ARUN KUMAR AND **MANISHA GUPTA** FROM JECRC UNIVERSITY IN JAIPUR, INDIA, PRESENT A UWB SYSTEM FOR NEXT-GENERATION MOBILE COMMUNICATIONS

Ultra wide band (UWB) uses a bandwidth of 500MHz, mainly for short-range and indoor communication. UWB channels operate in the range 3.1-10.6GHz with limited power density of -41dBm/MHz for indoor communication to avoid interference with other signals.

UWB communication was first used by the US military in the 1960s for applications such as radar and linking sensors. At present, there are two UWB network technologies: IEEE.802.15.13a, a standard for wireless personal area networks (WPANs) and the IEEE802.15.4a standard for ad-hoc communications.

Building A UWB System

To create a UWB system, it is necessary to understand the MAC and physical layers, which include a transmitter, receiver and channel.

There are two design approaches to building a UWB system: one is impulse-based with low data rates and no carrier; the other is MIMO-MB UWB (multiple input, multiple output, multiband UWB) where the available bandwidth is divided into a number of subcarriers to ensure high data rates and greater channel capacity.

Researchers have found that MIMO-MB UWB is most suitable for next generation wireless communication due to its many advantages, including high data rates, immunity to interference, low transmitting power and so on.

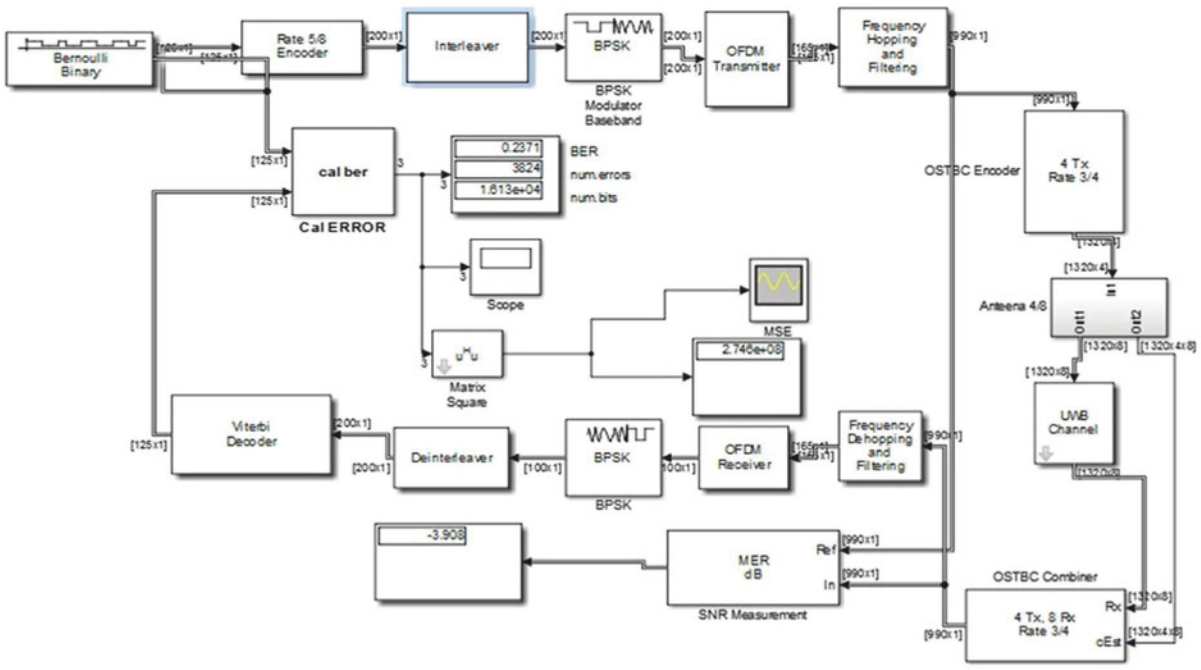

Figure 1: Proposed Methodology for UWB-BPSK

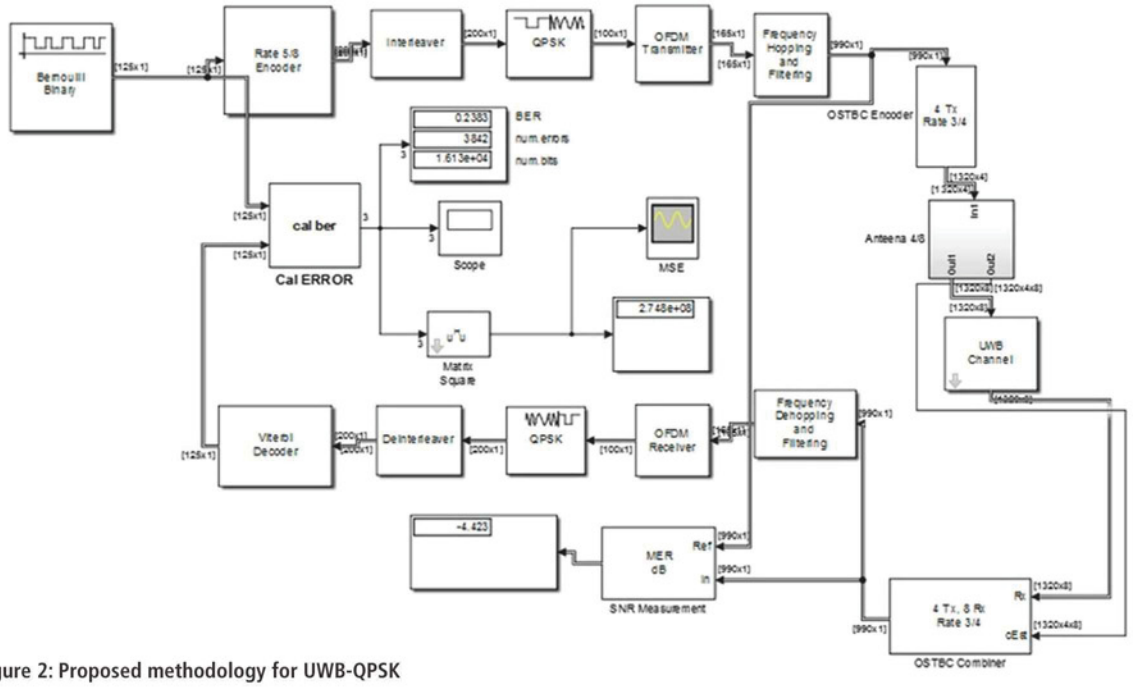

Figure 2: Proposed methodology for UWB-QPSK

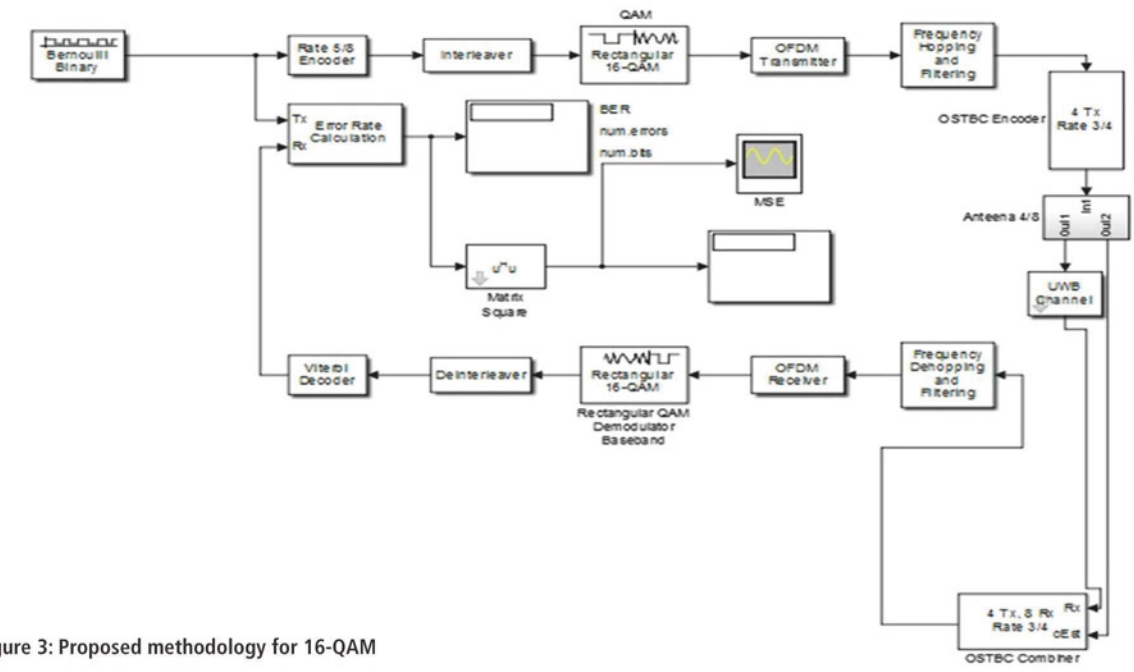

Figure 3: Proposed methodology for 16-QAM

A MIMO-MB UWB system is shown in Figures 1 to 5. Its input is generated using a Bernoulli binary generator, which prepares the binary numbers whose outputs are encoded at the rate of 5/8 by using punctured convolutional codes encoder. This type encoder concurrently processes multiple symbols whose output is sent to a matrix interleaver, which then interleaves the symbols by filling the matrix with input symbols row by row and sending the matrix content to the output port column by column. The output of the matrix interleaver is supplied to the modulator. The modulated output is then fed to the orthogonal frequency division multiplexing (OFDM) transmitter, implemented with a two-dimensional spreader. Cyclic-prefix (CP) is inserted

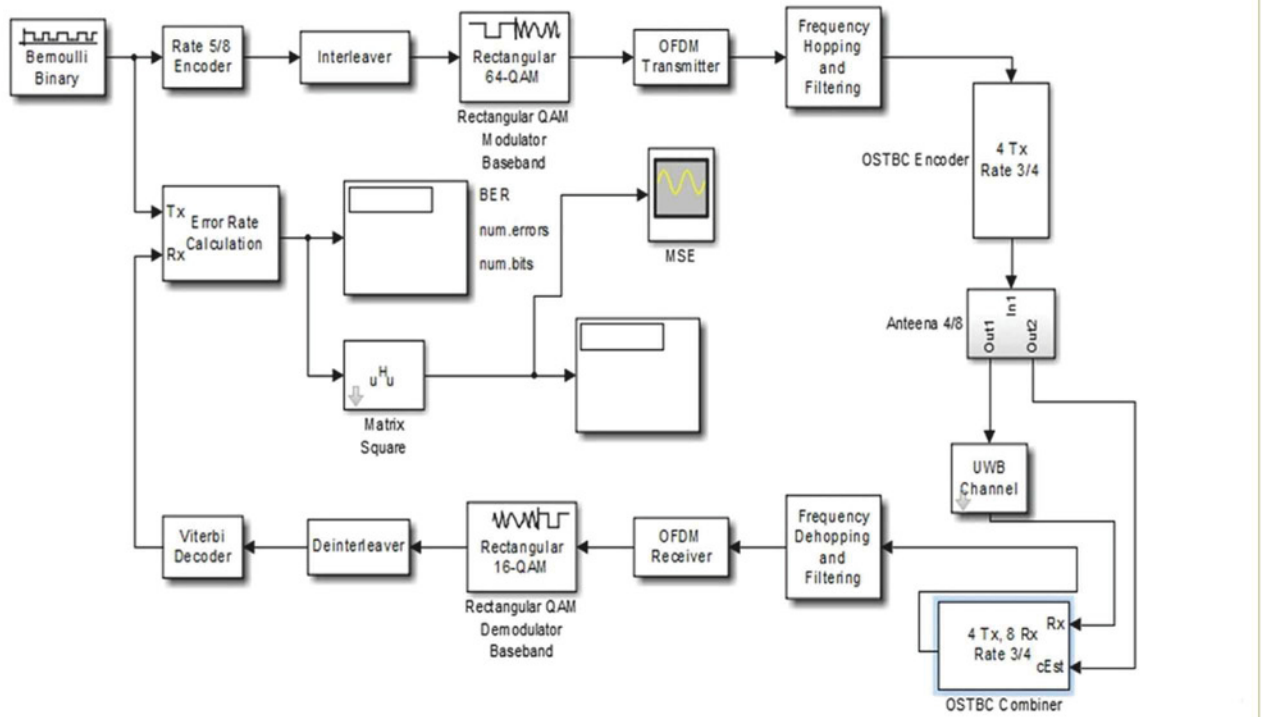

Figure 4: Proposed methodology for 64-QAM

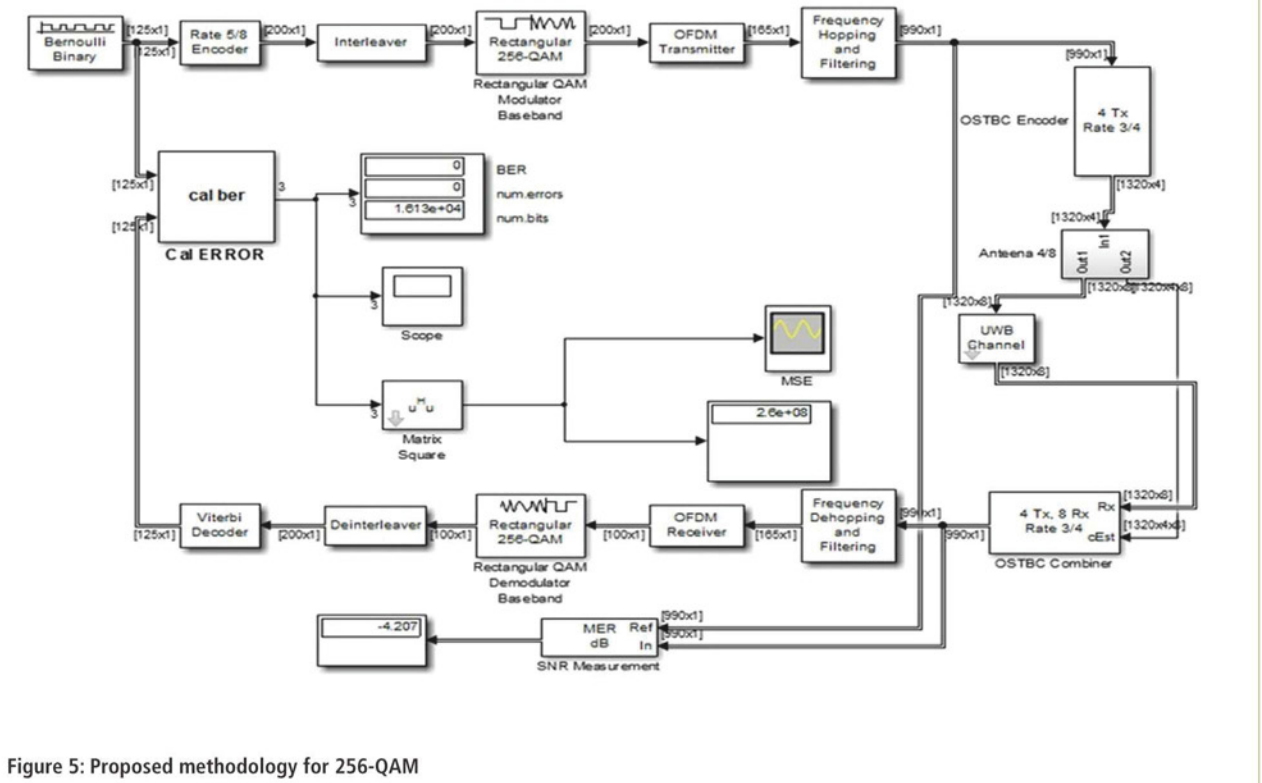

Figure 5: Proposed methodology for 256-QAM

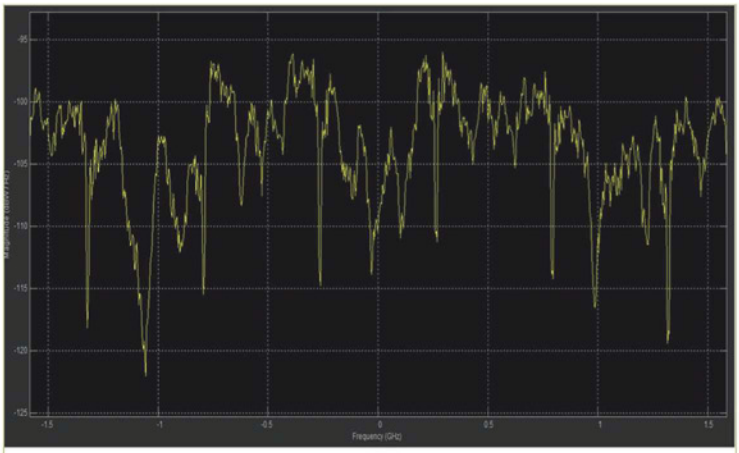

Figure 6: BPSK transmitted signal

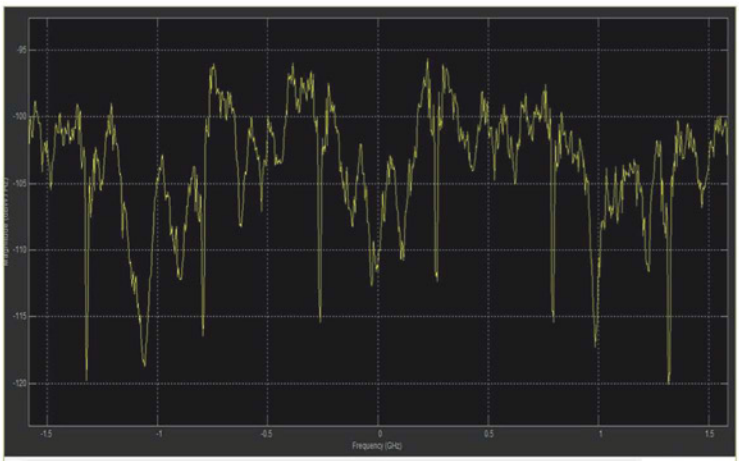

Figure 7: Transmitted QPSK signal

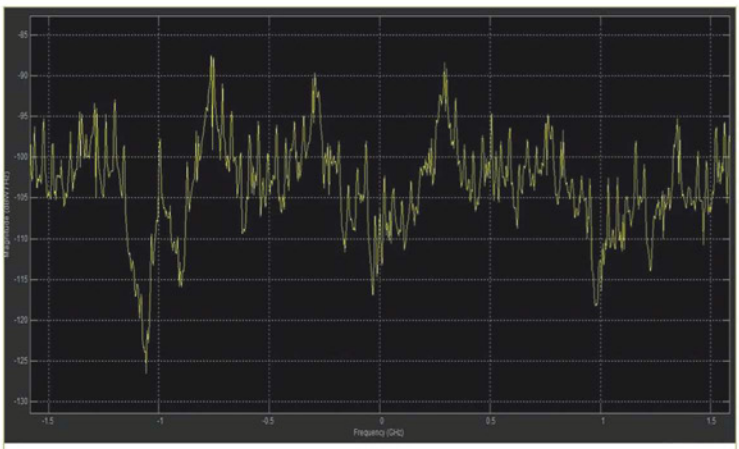

Figure 8: Transmitted signal for 16-QAM

between each symbol to reduce the effect of inter-symbol interference (ISI).

The Inverse Fourier Fast Transform (IFFT) of the signal is taken and sent to a frequency-hopping section and a digital filter. In the frequency-hopping module, the frequency is changed by switching to a different carrier, where the IIR digital filter allows a low frequency signal to pass. At the transmitter side, the input information is divided into several blocks. The OFDM signal transmitted by an Nth antenna is given by:

$$P(i) = \sqrt{\frac{E}{No}} \sum_{n=0}^{N-1} Xi(n) exp\ (j2\pi n\Delta f(t - \tau cp) \quad (1)$$

where $\Delta f = 1/T_F$. For MB-UBW OFDM, the transmitting antenna's signals are given by:

$$Yi(t) = \sum_{n=0}^{N-1} \{Re\{ S(t)(t - KJsys) exp\ (J2\pi Fct) \quad (2)$$

where Fc is the sub-band and KJsys denotes the number of bits transmitted during KJsys. The channel equation of the system is given by:

$$Z = Yn * Hn + n \quad (3)$$

where Y is the transmitted signal, H is the channel matrix and n is the noise.

The signal handled by four antennas at the transmitter end and eight antennas at the receiver end with addition of noise through the AWGN channel is given by:

$$Z_r = (h_{n.m} * Y_1 + n + pi + zf) * bn \quad (4)$$

where Z_r is the received signal
Y_1 = transmitted signal
n = noise
pi = Pilot symbol
zf = zero padding
bn = two-dimensional spread
h_{n*m} = channel matrix, where n is the number of transmitting antennas and m the number of receiving antennas.

At the receiver end, frequency 'de-hopping' and filtration are applied; the output is then fed to an OFDM receiver, where the pilot symbols, guard band and zero padding are removed and an FFT of the signal performed, given by the following equation:

$$R(k) = \sum_{k=0}^{n} Z(n) e^{-j2\pi Kn/N} \quad (5)$$

The signal is again diversified by a two-dimensional spreader. The demodulation that extracts the original signal from the modulated wave is given by Equation 6:

$$R(k) = \sum_{k=0}^{n} (Z(n) * Bn) e^{-j2\pi Kn/N} \quad (6)$$

Finally, a minimum-mean-square equalizer (MMSE) is used at the output, which reduces ISI. MMSE can be used only when the channel information and noise are accurately known; it reduces the mean square error of the signal which is given by:

$$MMSE = E\ \{(R\ (k)^* - R\ (k))^2\} \quad (7)$$

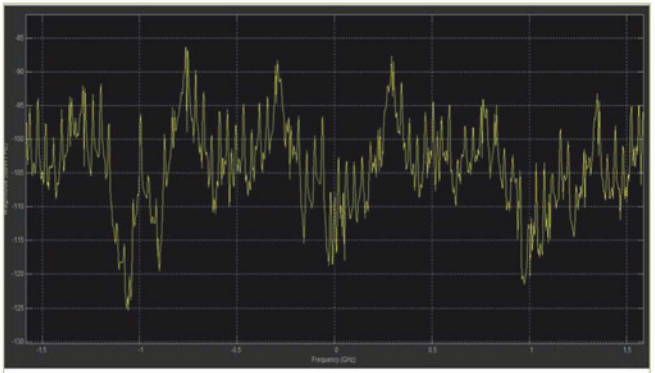

Figure 9: Transmitted 64-QAM signal

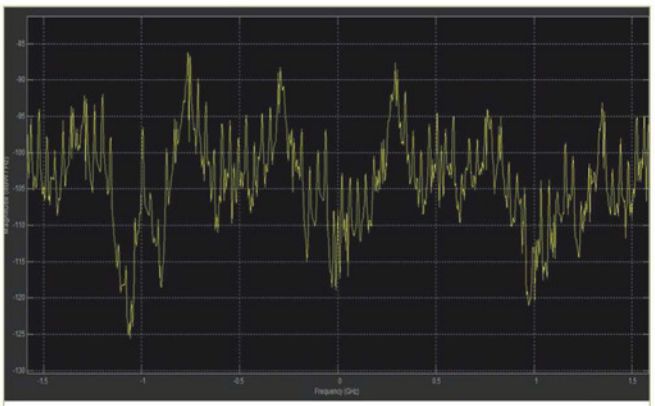

Figure 10: Transmitted 256-QAM signals

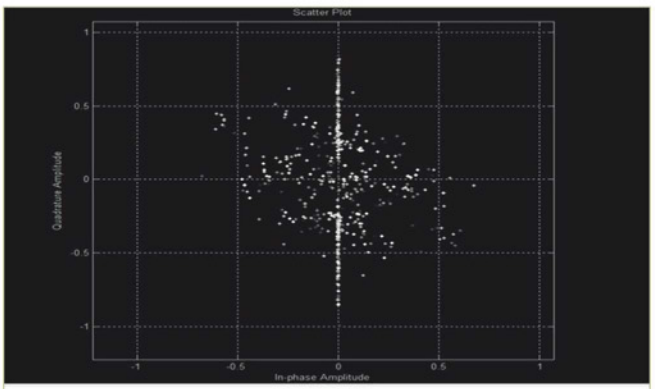

Figure 11: Received BPSK signal

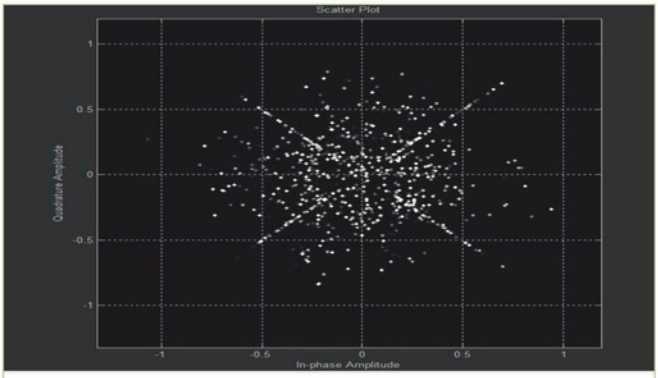

Figure 12: Received QPSK signal

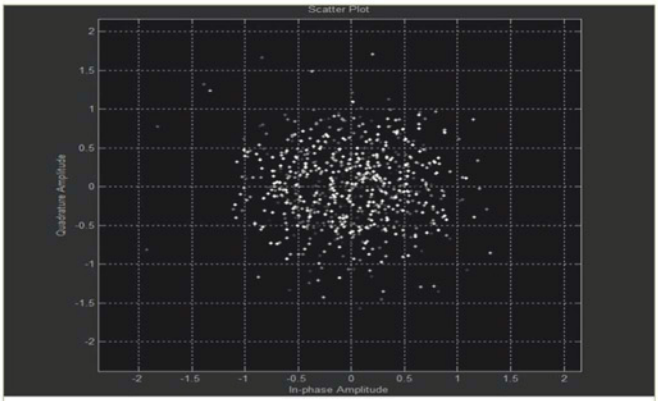

Figure 13: Received signal for 16-QAM

Performance Evaluation

The performance and efficiency of the system are evaluated on the basis of bit error rate (BER), constellation diagrams and MMSE plots for binary phase shift keying (BPSK), quadrature phase shift keying (QPSK), 16-QAM (quadrature amplitude modulation), 64-QAM and 256-QAM modulation schemes under CM1 LOS (line of sight) and CM2 N-LOS (non-line-of-sight) channel conditions.

The transmitted signals for the BPSK, QPSK, 16-QAM, 64-QAM and 256-QAM schemes are shown in Figures 6-10. The bandwidth used is 500MHz and each pulse is transmitted at a time period of 2ns. As shown in the figures, from 0-0.5GHz the transmitted pulse performance is good, and from 0.5-1GHz the transmitted signal is degraded, due to the transmission time being too short (2ns) to achieve synchronization between transmitter and receiver.

Constellation Diagram

The plot of quadrature vs in-phase amplitude is the constellation diagram. The constellation diagrams for the BPSK, QPSK, 16-QAM, 64-QAM and 256-QAM schemes are shown in Figures 11-15. From the results it can be seen that ISI is higher when the higher-order modulation schemes are used, compared to the low-order modulation schemes.

The equalizer plays a very important role in the higher-order modulation techniques for reducing ISI.

The plot of amplitude with time denotes the MMSE plot. It squares the input signal and produces a reduced error, which is useful for minimizing ISI.

BER

The UWB system's bit error rate for different modulation techniques is calculated for both LOS and N-LOS, as shown in Table 1. Overall, on the basis of BER, 256-QAM is the best candidate for a UWB system, where there are no obstacles between the base station and mobile handset based on LOS, and 256-QAM is the best candidate for a UWB system where there are no obstacles between the base station and mobile handset based on NLOS.

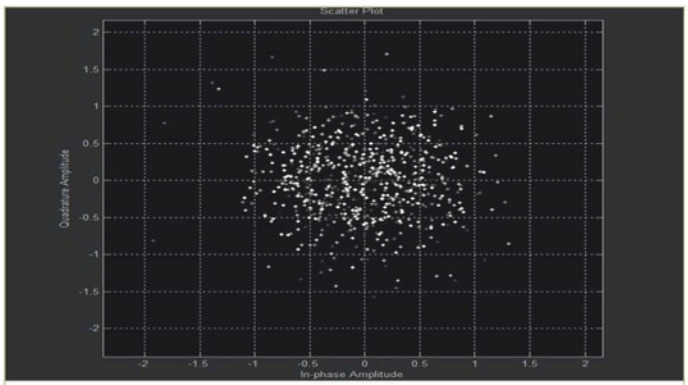

Figure 14: Received signal for 64-QAM

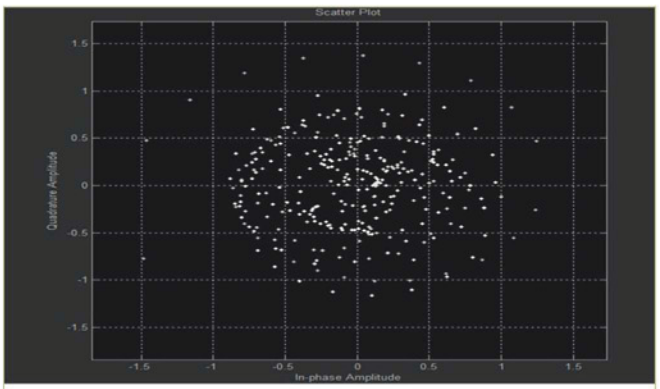

Figure 15: Received signal for 256-QAM

Future Work

The efficiency and performance of the proposed system was evaluated through CM1 LOS and CM2 NLOS channels (0 to 4 meters). From the simulated results and BER, we conclude that 256-QAM is the best modulation scheme for both CM1 LOS and CM2 NLOS channels.

Our results also reveal that the QPSK and BPSK modulation schemes are best suited for multipath environments; 16-QAM is well suited for a system that needs moderate data speeds; and higher-order modulation schemes, such as 64-QAM and 256-QAM, are best for a system that needs high data speeds and greater capacity, i.e. next-generation wireless communication systems.

UWB communication is also possible for longer distances, as it can generate data speeds up to 1Gbps by using 64-QAM, and more than 1Gbps by using 256-QAM; however, in this case the ISI effect will be much greater and an MMSE will be necessary to reduce it. Although an equalizer can't completely eradicate ISI, it can reduce it by reducing the conditions that cause it.

The efficiency of the MB-UWB system can be further improved by using efficient error-control coding techniques. ●

BINARY PHASE SHIFT KEYING (CM1 LOS (0 to 4 meters)														
Eb/No	-35	-30	-25	-20	-15	-10	-5	5	10	15	20	25	30	35
BER	0.2283	0.2295	0.2304	0.23	0.2308	0.2260	0.231	0.2235	0.2249	0.2269	0.2291	0.2371	0.2363	0.2293
CM2 NLOS(0 to 4 meters)														
Eb/No	-35	-30	-25	-20	-15	-10	-5	5	10	15	20	25	30	35
BER0.2367	0.2388	0.2390	0.2296	0.2372	0.2317	0.2308	0.2358	0.235	0.2341	0.2407	0.2449	0.2308	0.23	
QUADRATURE PHASE SHIFT KEYING (CM1 LOS (0 to 4 meters)														
Eb/No	-35	-30	-25	-20	-15	-10	-5	5	10	15	20	25	30	35
BER	0.2378	0.2392	0.2423	0.2450	0.2478	0.2419	0.2448	0.2414	0.2391	0.2420	0.2367	0.2376	0.2361	0.2352
CM2 NLOS(0 to 4 mete														
Eb/No	-35	-30	-25	-20	-15	-10	-5	5	10	15	20	25	30	35
BER	0.23	0.2410	0.2450	0.2517	0.2446	0.2451	0.2376	0.2393	0.2427	0.2479	0.2477	0.2484	0.2432	0.2410
16-QUADRATURE AMPLITUDE MODULATION (CM1 LOS (0 to 4 meter))														
Eb/No	-35	-30	-25	-20	-15	-10	-5	5	10	15	20	25	30	35
BER	0.43	0.4321	0.4345	0.4432	0.4473	0.4487	0.4595	0.4452	0.4412	0.4432	0.4354	0.4330	0.43	0.4294
CM2 NLOS(0 to 4 meter)														
Eb/No	-35	-30	-25	-20	-15	-10	-5	5	10	15	20	25	30	35
BER	0.4187	0.4231	0.4265	0.4278	0.4330	0.4362	0.4357	0.4497	0.4486	0.4387	0.4356	0.4321	0.4211	0.4232
64-QUADRATURE AMPLITUDE MODULATION (CM1 LOS (0 to 4 meter))														
Eb/No	-35	-30	-25	-20	-15	-10	-5	5	10	15	20	25	30	35
BER	0.4356	0.4832	0.4867	0.4921	0.4985	0.4965	0.4934	0.4914	0.4879	0.4884	0.4884	0.4897	0.4912	0.4977
CM2 NLOS(0 to 4 meters)														
Eb/No	-15	-10	-5	-4	-3	-2	-1	1	2	3	4	5	10	15
BER	0.4996	0.4976	0.4929	0.496	0.5013	0.498	0.4977	0.4929	0.4869	0.4866	0.4841	0.4871	0.4881	0.4897
256-QUADRATURE AMPLITUDE MODULATION (CM1 LOS (0 to 4 meter))														
Eb/No	-35	-30	-25	-20	-15	-10	-5	5	10	15	20	25	30	35
BER	0	0	0	0	0	0	0	0	0	0	0	0	0	0
CM2 NLOS(0 to 4 meters)														
Eb/No	-35	-30	-25	-20	-15	-10	-5	5	10	15	20	25	30	35
BER	0	0	0	0	0	0	0	0	0	0	0	0	0	0

Table 1: BER performance for the BPSK, QPSK, 16-QAM, 64-QAM AND 256-QAM schemes for LOS and N-LOS channels

ADVANTAGES OF DSPs IN THE DESIGN OF HI-REL, HIGH-OUTPUT POWER CONVERTERS

SOPHISTICATED DIGITAL POWER CONVERTERS PROVIDE KILOWATT-LEVEL POWER WITH CONFIGURABILITY AND REMOTE COMMUNICATIONS THAT ANALOG CONVERTERS LACK, SAYS **JEFF ELLIOT**

In the quest for better performance, flexibility, configurability, communications and remote monitoring and control, the power electronics industry is increasingly moving from analog to digital power converters, particularly when high-density power output is required.

Many mission-critical operations in aerospace and defence, as well as some industrial applications, require high-output power in the multi-kilowatts range. Given the mission-critical nature of these applications and the extremely rugged conditions in which they operate, these power converters must also withstand stringent vibration, shock, EMI, humidity and other environmental conditions without breaking down.

Meeting all these requirements often requires a custom solution from a power converter designer, proficient in digital signal processing (DSP) techniques as well as military and aerospace specifications and high-reliability (hi-rel) standards.

"You don't just go to a catalog and pick out something that's going to provide 50,000 watts of power. Almost everything is custom made in this space," says Kamran Kazem, Vice President and Chief Technology Officer at Magnetic Design Labs (MDL), maker of analog and digital switching and linear power supplies, DC-AC inverters and DC-DC converters.

Precise Control

According to Kazem, digital power devices operate over a very wide range, require few external components, are easy to communicate with, and allow a degree of control flexibility not available with analog techniques.

"The main reason to choose digital over analog is that almost anything can be customized fairly easily with just a little bit of code," says Kazem. "Whereas with an analog type of converter, once it is designed it is rather difficult to change or get any additional information from it, and there is no real-time communication."

DSPs are also far more precise than analog components. Settings do not drift, since they are controlled only by the DSP clock and the software, not capacitor or resistor values that change with temperature and time.

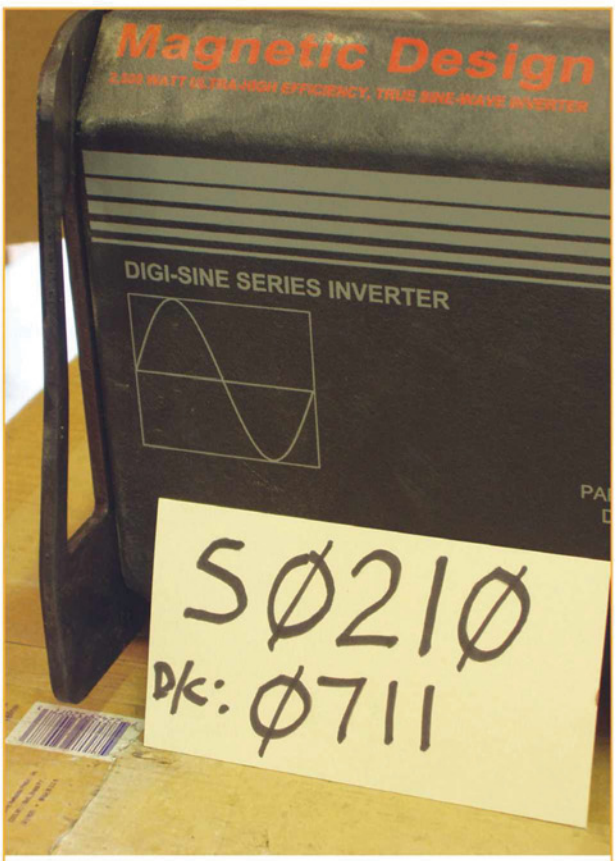

Figure 1: Many mission-critical electronics used in military and aerospace applications must be designed to satisfy stringent ruggedization and hi-rel requirements

"Perhaps the most important feature of a digital converter is its flexibility," adds Kazem. Digital power converters offer an array of programmable parameters, including output voltage settings, output current, current limit trip point, power sequencing routines, voltage margining and multiple thresholds for warning. There are fault conditions for overcurrent, overtemperature and under- and over-voltage, which can be stored in non-volatile flash memory for later recall."

Designers can program any of these parameters at any point during the product's lifecycle. These, as well as other function or feature changes, often simply require updating the flash memory, even remotely over the Internet. With analog, similar parameter or function changes require hardware changes and often a new PC board.

Learning Curve?

Real-time communication for monitoring and diagnostics is another major benefit. Digital power-conversion devices can be tied into existing networked systems, communication processors and software used to monitor and control the output.

Despite the advantages of DSP technology, for most engineers the major downside of digital power conversion is the learning curve the technology demands.

"It takes a very high skill-level and advanced education to successfully design for digital control of analog signals using a DSP," says Kazem.

He adds that despite excellent programming and debug tools from the DSP chip vendors, these tools can be very difficult for the inexperienced designer.

"Designers used to working in the analog domain can get into a sophisticated DSP application and find that it takes too long or becomes too difficult to complete the work," he added.

Hi-Rel Applications

In addition to DSPs, many mission-critical electronics used in military and aerospace applications must be designed to satisfy stringent ruggedization and hi-rel requirements.

Hi-rel is defined as the probability of failure-free performance under stated conditions, usually over a specified interval. These systems, down to the component level, must be able to operate for many years without failure, often without the possibility of repair, and have to operate in temperatures from -55C to +85°C.

> High-reliability electronic systems and components are no longer the exclusive domain of aerospace and defense

Bob Seidenberg, former Senor Quality Assurance Manager with BAE Systems, describes the importance of the digital inverters that were installed in the M1068, a Command Communications variant of the US Army's M113 family of armored personnel carriers. BAE Systems is a global defence, security and aerospace company that designs and manufactures electronic systems and subsystems for commercial and military applications.

The original M113 Armored Personnel Carrier (APC) revolutionized mobile operations when first used in Vietnam. To date, an estimated 80,000 M113s, including a long list of variants, have been produced and used by over 50 countries worldwide, making it one of the most widely used armored fighting vehicles of all time.

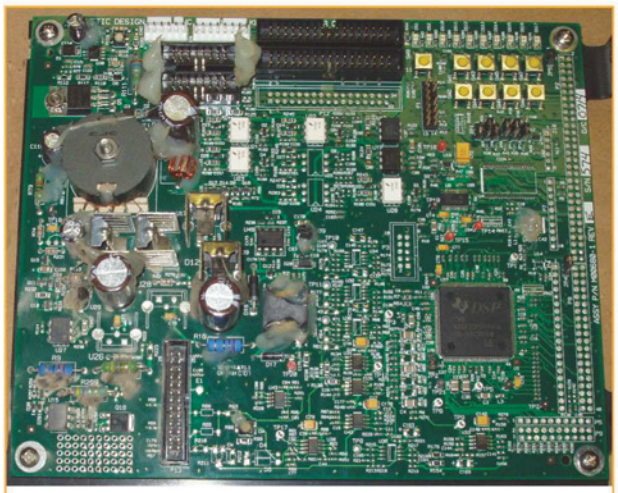

Figure 2: Pure-sine-wave inverters are ideal when operating sensitive electronic devices, including communications equipment, that require a high-quality waveform and low harmonic distortion

The M113 has been updated over the years to meet the ever-changing demands of the modern battlefield. Since then, the M113 family is being upgraded, reconfigured and introduced as entirely new systems, including the M1068. The M1068 variant is used as a tactical operations centre capable of long-range communications, and includes 4.2kW auxiliary power unit (APU) mounted on the front of a vehicle to provide 24V power.

As part of this project, BAE Systems required two hi-rel, ruggedized 2500W pure-sine-wave inverters per vehicle to convert the APU-generated 24V DC power into usable multi-kilowatts of AC for powering communications, lighting, computers and other electronics.

Although more expensive, pure-sine-wave inverters provide cleaner utility grade power than quasi-sine-wave models. Pure-sine-wave inverters are ideal when operating sensitive electronic devices, including communications equipment, that require high-quality waveform with little harmonic distortion.

In addition, pure-sine-wave models have a high surge capacity and can exceed their rated power for a limited time. This enables vehicle motors to start easily, which can draw many times their rated power during startup.

Seidenberg explains that the 2500W inverters also meet some shock and vibration requirements that could only be met by hi-rel inverters.

"The shock requirement for the inverters installed on the M1068 was close to 30Gs in all three directions, and the vibration spectrum was also very demanding, but MDL was able to meet those requirements with an innovative pure-sine-wave inverter design that was basically non-destructive," says Seidenberg.

According to MDL's Kazem, despite the 30G requirement for the M1068, the military specified that the inverters had to withstand 100Gs. This was well beyond the amount of shock the

vehicle would ever realistically experience, based on military tests conducted in the roughest terrain that maxed out at 15Gs. Still, MDL was able to deliver 2500W, pure-sine-wave inverters that met the requirements, as verified by an independent testing lab.

"The military has a number of requirements we had to follow," says Seidenberg. "So naturally, our supplier had to pay a lot of attention to those requirements and ensure they were met in a correct way for the application."

Kazem adds that high-reliability electronic systems and components are no longer exclusive to aerospace and defense. Today, medicine, transportation, communications, infrastructure and industry all have applications where the price of failure is high.

"These power converters might not have to withstand the same extreme conditions as the military, but vibration, shock, humidity and other inherent environmental problems are still factors, so the need for hi-rel and rugged power converters certainly applies to those markets as well."

Stackable Inverter Modules

The DSP is also a key element in a new generation of modular, stackable inverter options, designed to provide a range of 1-20kW of DC-AC power via a single, customizable unit. This type of system, available from custom power converter designers like MDL, consists of rack-mounted inverter modules that can be stacked in parallel, enabling the user to add as many inverters as needed. Each unit connects to a communications controller, and handles synchronization, load sharing and external communication. The individual inverters are hot-swappable, enabling the addition or replacement of modules on the go.

"This type of modular design provides project managers with a system that fits their power requirements without having to develop a new unit just for their specific project," says Kazem. "This eliminates the need for many application-specific designs and could also enable faster delivery of the power converter much more economically."

NEW DIRECTORS AND NEW STRUCTURE AT SPEEDBOARD

Contract electronics manufacturer (CEM) Speedboard Assembly Services has appointed Martin Bullimore as its Operations Director. Bullimore has an electromechanical background and 30 years of manufacturing experience, having worked for a number of market-leading OEMs, including Nokia, Stannah and Alexander Dennis. In his new role, Bullimore will be responsible for the day-to-day running of Speedboard's production and engineering activities, as well as overseeing all final assembly and test activities.

Speedboard has also promoted Karen Heath from Commercial Manager to Supply Chain Director. Prior to joining Speedboard in 2007, Heath held positions with Delta Impact and Macro, which subsequently become part of Avnet. In her new role, Heath's new responsibilities include managing supplier quality, supply strategies, the timeliness of deliveries, purchasing and stores.

These appointments come amidst other organisational changes at Speedboard.

www.speedboard.co.uk

MULTIFUNCTION TESTER ENSURES STANDARDS COMPLIANCE

Advanced-technology electrical testing equipment is helping a specialist manufacturer of electrical wiring harnesses and control panels for diesel engine applications demonstrate compliance with rigorous industry standards. The North East manufacturing operations of CMR UK have extended its electronic control panel test capability with the purchase of a new Seaward HAL 104 multi-function electrical safety tester.

The HAL 104 combines the performance of a multi-function production line safety tester with load and power factor measurement for component and assembly energy consumption and ratings assessments.

Incorporating AC/DC Hipot (flash/dielectric strength), the tester can perform load and power functional tests, insulation, ground/earth bond testing to 40A, load testing to 16A with leakage measurement to 20mA.

The new tester is provides HV dielectric testing and insulation resistance measurement on panel assemblies to endure electrical safety standards compliance.

www.seaward.co.uk

EXCEPTION EMS EXPANDS CAPACITY AND TECHNICAL CAPABILITIES

Exception EMS, the UK-based contracts electronics manufacturing solutions provider, has recorded 2015 as the year with highest ever turnover in its history, as it continues to grow its business into key vertical sectors including telco, energy and defence. The company also recently invested over £2m in two new SMT lines that will see it expand its capabilities and capacity.

"Year 2015 has once again exceeded our goal, with a record turnover of around £22m and growth of over 40% in our on-demand business," said Mark O'Connor, Exception EMS CEO. "While we continue to grow our business, we continue to provide our customers with a service that is second to none, and meet all their requirements in the challenges they face in terms of technical innovation."

The two additional lines are based on the Siemens/ASM SX platform, with three SX machines configured in one line and two SX machines in the second line. There are also new DEK Horizon temperature and humidity controlled printers, 3D solder paste inspection from Koh Young, Rhem 14 zone reflow ovens and AOI from Cyberoptics, giving the lines leading edge specification from end to end.

www.exceptiongroup.com

HAND-SOLDERING COMPETITION

Coming back to the NEC is the IPC Hand-Soldering Competition in association with Advanced Rework Technology, returning to National Electronics Week from 12th-14th April 2016. There are cash prizes and a ticket to SMT Nuremberg 2017 for the winner who will pit their skills against an international pool of experts.

Participants will compete to build a functional electronics assembly within a 45-minute time limit. Assemblies will be judged on soldering in accordance with IPC-A-610F Class 3 criteria, the speed at which the assembly was produced and overall electrical functionality of the assembly.

If interested in competing this year, contact:

marketing@neweventsltd.com

ATMEL ACHIEVES INDUSTRY'S FIRST AUTOMOTIVE SPICE LEVEL 3 CERTIFICATION

Atmel announced that its maXTouch firmware development facility in Whiteley, the UK, has achieved the Automotive SPICE Level 3 certification that addresses rigid requirements for software development processes for tier 1 and tier 2 partners in the automotive industry.

SPICE, also known as Software Process Improvement and Capability dEtermination, is a process assessment model with a set of technical standards documents for the computer software development process and related business management functions. It is one of the joint International Organization for Standardization (ISO) and International Electrotechnical Commission (IEC) standards, and it was developed by the ISO and IEC joint subcommittee ISO/IEC JTC 1/SC 7. Automotive SPICE is a version that applies specifically to the automotive industry, however its benefits will also apply to the consumer and other industries that may use maXTouch technology.

To achieve the certification, Atmel redefined and redesigned its software development process over a three-year period. Atmel achieved Automotive SPICE Level 2 compliance in 2014, and Level 3 after the final independent assessment was completed at its Whiteley facility in November 2015.

www.atmel.com

ELM EV ADOPTS NEW TEST TECHNOLOGY

Elm Electric Vehicle Charging Solutions has become one of the first companies to use a new test technology for fast and efficient fault-finding and maintenance of charging installations.

Its new EV100 test instrumentation was developed by Seaward for comprehensive validation testing and fault finding on all types of AC electric vehicle charging equipment. Elm is independent electric vehicle supply equipment (EVSE) company, responsible for over 2,000 charging-point installations for private and public sector clients throughout the UK.

For diagnostic testing, the dedicated EV100 tester simulates several different vehicle faults and measures the EVSE response, including disconnection time and the amplitude, frequency and duty cycle of the PWM signal. Tests and maintenance schedules are done automatically and in accordance with IEC 61851.

www.seaward.co.uk/EV100

THERMACORE SHOWS HEAT TRANSFER TECHNOLOGY AT IMAPS

Advanced heat transfer technology is on show at the International Microelectronics Assembly and Packaging Society's (IMAPS) event by leading thermal management solutions company Thermacore Europe. The IMAPS workshop on micropackaging and thermal management is in La Rochelle, France, on the 4-5 February.

Thermacore's k-Core features encapsulated Annealed Pyrolytic Graphite (APG) to provide rapid, reliable and effective high-conductivity thermal spreading for a wide range of heat transfer and cooling applications in the aerospace, transportation and defence sectors.

Samples of the technology, which provides up to three times the conductivity (k) of solid copper with lower mass than aluminium, will feature as the centrepiece of the company's presence at IMAPS, where Mark Small, Thermacore's area sales manager, will be presenting a paper to delegates on APGs.

www.thermacore.com

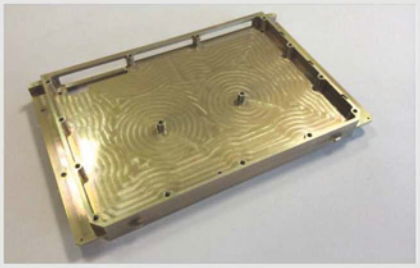

RIGEL 62353 PLUS MEETS MEDICAL DEVICES' TEST NEEDS

Rigel Medical has introduced an upgraded version of its dedicated tester for the in-service and post-repair safety testing of medical electronic devices in line with the standards required by IEC 62353.

In sync with changes in test requirements from manufacturers of 24V DC and 48V DC operated medical equipment, such as operating tables and portable lighting installations, the new Rigel 62353 Plus tester is equipped with an extended range of insulation test voltages between 50V DC to 500V DC.

As a result, four separate insulation test voltages are now provided at 50V DC, 100V DC, 250V DC and 500V DC to give the latest tester even more flexibility in meeting the routine safety testing needs of medical devices in tune with the internationally recognised in-service test standard.

www.rigelmedical.com

CONTACTLESS, PROGRAMMABLE ANGLE POSITION SENSOR IC

The A1335 from Allegro MicroSystems Europe is a new 360°, contactless, high-resolution, programmable, magnetic, angle position sensor IC designed for digital systems in automotive and related applications that involve rotating shaft sensing.

The A1335 is a system-on-chip (SoC) with a front-end based on circular vertical Hall technology and incorporating programmable microprocessor-based signal processing. It supports multiple communication interfaces including I2C, SPI (Serial Peripheral Interface) and SENT (single edge nibble transmission).

The A1335 also provides two options for on-chip linearization: harmonic, to handle applications that require side-shaft magnetic configurations, and segmented, for scaling angle measurement applications requiring less than 360° motion (so-called "short stroke" applications). The on-chip EEPROM supports up to 100 read/write cycles for flexible programming of calibration parameters.

www.allegromicro.com

HIGH-SENSITIVITY CURRENT PROBES FOR YOKOGAWA OSCILLOSCOPES

Two new high-sensitivity current probes are now available for Yokogawa's families of mixed-signal oscilloscopes and ScopeCorders.

The 701917, covering a frequency range from DC to 50MHz, and the 701918, covering DC to 120MHz, offer sensitivities ten times higher than previous models (typically 1V/A) along with low noise levels of typically 60µA RMS. They are ideally suited for measuring low-level currents from about 1mA to 5A.

The probes feature a slim, lightweight sensor-head, which is easy to use in confined spaces. Automatic zero adjustment and demagnetisation are accessed via a button on the termination box, making setup quick and easy. An overload/jaw-unlocked warning is included for added safety.

The instrument connects via the front-panel BNC. Power can be provided from the oscilloscope's probe or a separate power supply.

tmi.yokogawa.com

KYNAR EDUCTOR NOZZLES MEET THE CHEMICAL CHALLENGE

Storing liquids in tanks is essential for many process industry applications, for example chemicals for finishing and surface treatment applications, as is the need to agitate the contents to avoid separation and sedimentation. Fluids can be re-circulated through tanks to achieve separation which helps to optimise chemical action in dip tanks, although the process can be enhanced by the introduction of eductor nozzles.

For many applications, eductor nozzles made from brass or stainless steel (as opposed to plastics such as polypropylene) are the preferred choice, especially if the chemicals are aggressive, or are stored at higher temperatures. However, the new range of PVDF eductors, recently introduced by BETE is a viable alternative to the more expensive stainless models. PVDF (Kynar) is an incredibly chemically-resistant fluoroplastic and has superior heat resistance compared to many other plastics.

www.bete.co.uk

HORIZONTAL GECKO CONNECTORS REDUCE PCB STACKING HEIGHT

Harwin has introduced a horizontal version of its 1.25mm pitch hi-rel Gecko connector, reducing the stacking height of PCBs to just 5.6mm. Available in the standard eight positions of 6, 10, 12, 16, 20, 26, 34 and 50, the new style also facilitates mother- and daughterboard configurations.

G125 series connectors offer high performance in a miniature package. The 1.25mm pin spacing results in a 35% space-saving over other high-performance connectors such as Micro-D. Connectors can handle 2A per contact and function within a wide temperature range (-65 to +150degC) and under extreme vibration (Z axis 100g 6m/s).

Other features common to the Gecko connector family include polarization points that prevent mis-mating, easy identification of the No 1 position for fast visual inspection and optional latches that allow simple and fast de-latching.

www.harwin.co.uk

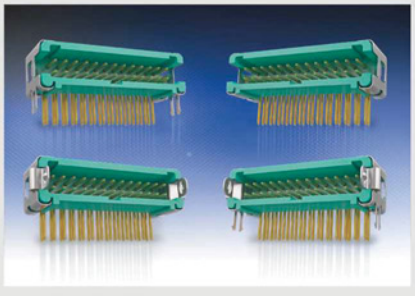

PANASONIC PAN9320 EMBEDDED WI-FI PLACE-AND-PLAY MODULES NOW AT MOUSER

Mouser Electronics is now stocking the PAN9320 embedded Wi-Fi place-and-play module from Panasonic. This fully-embedded Wi-Fi module features an integrated stack, full security suite and API to minimize firmware development. The PAN9320 device is a standalone 2.4GHz Wi-Fi module that supports the IEEE 802.11 b/g/n standards, designed for applications where a small form-factor and high-throughput data rates are required. The PAN9320 module provides a cost-effective, power-efficient solution for WLAN applications.

The Panasonic PAN9320 module combines a high-performance CPU, high-sensitivity (-98dBm) wireless radio, baseband processor, medium access controller, encryption unit, boot ROM with patching capability, internal SRAM and in-system 1 Mbytes programmable flash memory.

The PAN9320 module includes a coincident support for access and infrastructure modes, enabling use in smart devices and home network routers simultaneously.

www.mouser.com

DRAMATICALLY IMPROVED CHARGING PERFORMANCE WITH INNOSWITCH-CP ICS

Power Integrations launched the InnoSwitch-CP family of offline CV/CC flyback switching ICs that incroporate a constant power output profile. This feature, when paired with an adaptive-voltage protocol such as Qualcomm Quick Charge 3.0 or USB-PD, enables OEMs to optimize the charging time across a whole host of smart mobile products.

Developers employing adaptive charging technology achieve dramatically faster charge times, improved charging efficiency and backward compatibility with the popular 5V USB BC 1.2 specification, whilst minimizing overall thermal management and costs.

InnoSwitch-CP ICs use Power Integrations's innovative FluxLink technology which enables high-performance secondary-side control to be implemented with the simplicity and low component-count usually associated with primary-side regulation. FluxLink technology also optimizes the effectiveness of output synchronous rectification, resulting in extremely high efficiency across the full load range.

www.power.com

HARTING'S HANONBOARD TECHNOLOGY ALLOWS POWER CONNECTION DIRECTLY ONTO THE PCB

HanOnBoard is a connector technology from Harting that can replace standard discrete wiring by allowing power I/O connectors to be mounted and connected directly onto the printed circuit board (PCB).

With the HanOnBoard concept, Han connectors are connected to the board via a PCB mounted adapter through which data, signals and power are distributed. This solution eliminates time-consuming and potentially fault-prone wiring and is based on an optimum combination of tried-and-tested Han components, Harting PCB adapters and Harting PCB solutions.

Due to HanOnBoard's compact and weight-saving features, it offers additional benefits over traditional wiring: PCBs are more resistant to external influences such as shock and vibration compared with discrete wiring, and the total electrical path can be conformally coated to provide enhanced protection, suitable for harsh environments.

www.harting.co.uk

AMPHENOL ENHANCES STANDARD SHELL PLATING ON CONNECTORS

Amphenol Industrial Products Group, a global supplier of interconnect systems, has enhanced its standard shell plating from standard cadmium to gray zinc over electroless nickel (Gray ZnNi) for use in the harshest environments. Initially designed for marine applications, this plating is now found in military and industrial applications and/or where RoHS-compliant plating is required.

Amphenol's upgraded, cadmium-free connector offers high corrosion resistance and no significant galvanic reaction when mated with leading standard market plating options.

Compatible with market standard plating options, Gray ZnNi is non-magnetic so it can be used safely in magnetic environments in conjunction with another non-magnetic connector shell. Its operating temperature range is -65°C to 200°C and another of its features is the 500-hour salt spray rating.

www.amphenol-industrial.com

NEW, SMALL-SIZE, GORE ACOUSTIC VENT GAW333

W. L. Gore & Associates launched its GORE Acoustic Vent GAW333 – a smaller, smarter way to improve mobile phone acoustics while maintaining IPX8 immersion protection and IP6X particle protection.

With inner diameter of just 1.5mm, the new GAW333 packs a lot of performance into a very small vent, to offer greater design flexibility to mobile phone developers. It delivers robust sound performance, with the lowest acoustic attenuation of any IPX8 GORE acoustic vent. As measured with a MEMS microphone system, a GAW333 vent with an inner diameter of 1.8mm exhibits very low transmission loss: typically around 2dB at 1kHz.

The advanced microporous structure of this GORE membrane rapidly and reliably equalizes pressure differentials, while remaining virtually impenetrable to water, dirt and debris. It withstands extended immersion at 2 meters for 1 hour.

www.gore.com

HIGH-FREQUENCY 600MA DC-DC BUCK CONVERTER FOR HIGH EFFICIENCY

Targeting mobile phones, wearable devices and similar battery-powered applications, the AP3405 DC-DC buck converter introduced by Diodes Incorporated delivers high efficiency under light and heavy loads. Operating with a fixed switching frequency of 2MHz it reduces the size of external components while its small U-DFN2020-8 package also saves board area.

The AP3405 current mode, PWM synchronous, step-down converter operates with a 2.3-5.5V VIN range and supplies an output from 0.7-5.5V, accurate to ±1.5%, up to 600mA. A low quiescent current draw helps extend battery life and internal MOSFETs with low RDS(ON) enable high efficiency under all load conditions.

Comprehensive protection features built into the AP3405 protect both the end system and the device itself. These include hiccup mode short-circuit protection (SCP), under-voltage lock-out (UVLO), over-temperature protection (OTP) and over-current protection (OCP).

www.diodes.com

Ever pressed **Shift + 4** on a keyboard?

We have.
It's $YFN.

As you see... everything is connected.

4YFN
CONNECTING STARTUPS

22-25 February 2016
Barcelona, Spain

Join us in February at the fastest growing technology startup event in the world, **4YFN at GSMA Mobile World Congress** held in Barcelona.

For more information, visit www.4yfn.com/MWC

#4YFN

Lab Partner
IBM

Silver Partners
ITRI Industrial Technology Research Institute
Weigo | CITY

Gold Partners
Sabadell BStartup
Telefónica OPEN FUTURE_

Bronze Partners
FUNDACIÓ puntcat
nominalia

Founders & Investors Partner
La French Tech
Powered by BUSINESS FRANCE

An event of
MOBILE WORLD CAPITAL BARCELONA
GSMA MOBILE WORLD CONGRESS